Possibilities and Challenges in Temporal Control of XUV Pulses by Opto-optical Modulation

Anna Olofsson

Thesis submitted for the degree of Master of Science
Project duration of 4 months

Supervised by
Johan Mauritsson and Samuel Bengtsson

LUND UNIVERSITY

Department of Physics
Division of Atomic Physics
May 2018

LRAP 549

Abstract

Recent developments in opto-optical modulation technique calls for improved temporal control of light modulation processes of coherent XUV light. This thesis project evaluates an experimental method aimed at achieving redirection and amplitude modulation of XUV-light, by using precise determination of decay times in states of noble gases that are deemed suitable for opto-optical control. It is possible to obtain a higher signal-to-noise ratio than previously possible when performing decay time measurements using a recently developed technique to obtain spatial phase control of the states that are being measured.

Acknowledgements

Many thanks to my supervisors, who spent countless hours in the lab with me. I would also like to thank the rest of the Attosecond XUV Spectroscopy group and my office mates - if ever a laughter escaped you at a mistake I made, you managed to always keep it goodhearted and kind. Thanks are also due to my friends and family, who kept my spirits up with a never-ending stream of encouragement and German oxygen-blasting plants.

Contents

1 Introduction

Nearly thirty years ago, the wide field of spectroscopy suddenly changed in a significant way: the short pulses created by the first Kerr lens mode-locked titanium sapphire laser pushed the temporal resolution of spectroscopy into the femtosecond regime, which opened up the possibility of detecting and analyzing chemical processes on their natural timescale [1]. However, the majority of the electron cloud dynamics were still hidden due to the short interaction time and the fact that any light used to study them would in general need to be in the extreme ultraviolet (XUV) regime [2]. Before the 1990's, there were no coherent tabletop XUV-sources, making this requirement a difficult one to fulfill [1]. The advent of High-order Harmonic Generation (HHG) changed this fact, and now tabletop XUV sources are available. Furthermore, HHG produces pulses with pulse durations shorter than any previous man-made event; HHG can deliver coherent pulses with pulse durations below 100 attoseconds [1][3][4]. As of today, there exists an ambition within the field of ultrafast optics to reach pulse durations in the zeptosecond regime [1], which could offer an even better temporal resolution and higher peak intensities than what can be reached with attosecond pulses.

The possibilities offered by the development within ultrafast optics span many different research fields and industry applications. One industry, which perhaps is the industry that has profited the most from ultrafast optics, is laser materials processing, which utilizes ultrashort pulses to obtain cold ablasing [1]. Cold ablasing is a form of laser etching that uses the high energy and short pulse duration of ultrashort laser pulses to obtain multi-photon processes in a thin layer of material. This technique offers the possibility of changing the material from solid form to gas form directly without heat transfer and damage to the surrounding material [1]. This gives a high-precision, material-specific etching that can be used for example to cut sensitive material or to create optical waveguides. However, ultrashort pulses require special optical components since the high peak intensity of an ultrashort pulse can easily damage the optics [1]. This is a problem for both the development of solid state ultrafast lasers and the spatial precision of ultrashort laser material processing. For these applications to reach their full potential, opto-optic modulators (OOM) and all-optical beam splitters are hypothesized to be of great assistance [1].

Another possible application for ultrafast technology where there is an interest for an OOM is ultrafast communication and signal processing. These two research and industrial fields seems to be constantly growing and improving, with an ever-present need for speed-ups. This is why they have started investigating the possibilities of ultrafast optics. However, if any real progress is to be made, optical components and control mechanisms compatible with higher speed and intensity need to be developed [1].

Ultrafast optics has also affected several other research fields, for example theoretical physics, biology, chemistry and meteorology. The effect on biology and chemistry lies in the possibility to image chemical processes on their natural timescale: for example, charge tracking in molecules is believed to advance the understanding of chemical structural changes in reacting molecules [1]; another example is that HHG offers light in the frequency region that is needed to study bound states in atoms and molecules [2]. Ultrafast optics might also make it possible to study decay processes more carefully and evaluate the effect of dephasing

and macroscopic processes on decay times of atoms and molecules, an area where time-resolved spectroscopy seeks more knowledge [1].

The list of the fields where ultrafast optics may be of use could be made significantly longer, but these are the fields where the progress seems tangible and likely. They also share another trait; researchers in these fields request increased spatial or temporal control of ultrafast light, and highlight the difficulty of working with standard optical components [1]. These problems may have a solution in the OOM, that could be used to decrease the difficulty of controlling and steering XUV light [5]. It is not strange that the idea of an OOM is so tempting; its acoustic counterpart, the acousto-optic modulator (AOM), that operates on longer timescales, is used in so many different areas that it is not possible to mention all of them here. A couple of examples are laser scanning, nonimpact printing, color separation, medical x-ray digitizing and reconstruction, large screen television displays, measuring dopant levels of wafers, medical surgery procedures, dental procedures and laser heterodyne meteorology, just to mention a few to give insight into the wealth of applications of the AOM [6]. Given the success of the AOM, it is no surprise that both hopes and expectations are set high should an OOM be developed.

The process of developing an OOM is ongoing; in an article published in 2017, a technique for redirecting XUV light using HHG and attosecond pulses is described [7]. In other words, the article proved that spatial steering of XUV light using an ultrashort pulse of infra-red (IR) light is possible. Hopefully, this can serve as the spatial control needed for an OOM. However, spatial control of light is not the only trait needed to create the OOM; amplitude control is also needed, and preferably also phase control. The amplitude control is what this thesis project is focused on. The amplitude control method that is investigated in this thesis is built upon the spatial control from [7], and the spatial control will therefore be discussed at length in succeeding sections of this report. In short, this thesis investigates a proposed method to modulate the amplitude of XUV light by measuring decay times for the atomic states used in the redirection process, in order to obtain a calibration of the redirected fraction of the light depending on the timing of the redirecting IR pulse. This reasoning follows from the fact that the atoms will emit energy in the forward direction until the attosecond IR pulse interacts with the atoms and causes the emission to change direction.

The decay time measurements and the strive for an OOM form a symbiosis: the decay time measurement could push the OOM technology forward, while the decay measurements use the existing spatial redirection to improve the precision of decay measurements. The possibility for improvement originates in the spatial separation of the decay signal from the transmitted radiation, which could result in an improved signal-to-noise ratio (SNR) [7] since the transmitted radiation in current measurement methods acts as noise and is usually significantly brighter than the signal. An improved SNR and the tabletop XUV-light pulses made obtainable by HHG could make it easier to investigate the pressure dependence of the decay time, and investigating the dephasing and macroscopic processes involved at different pressures - which would serve both the OOM-technology and the needs of the field of time-resolved spectroscopy.

2 Theory

In the following section, the theoretical concepts necessary to understand the proposed method for intensity control of optical modulation is presented. The foundation of the method is based on light-matter interaction, and therefore it is in basic light-matter interaction this section will begin. The section will then delve deeper into more advanced light-matter interaction that explains how an absorption process can be modulated and steered.

2.1 The decaying dipole picture

The decaying dipole picture is an approximation used to describe the fundamental light-matter interaction of absorption and emission of photons by atoms. The absorption of a photon has historically often been described as instantaneous. This is, however, not true. A more accurate picture is instead that of the decaying dipole with a short decay time that may be short. The dipole picture can be described as follows: when an atom interacts with an oscillating electric field, the positive nucleus experiences a force in a direction parallel to the direction of the field, while the negative electron experiences a force that is in the opposite direction to the direction of the field. This creates an atomic dipole moment as shown in Fig. 1.

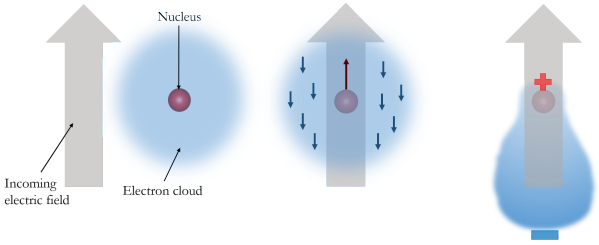

Figure 1: Schematic description of the interaction picture between an atom and an incident electric field. Due to the positive charge of the nucleus and the negative charge of the electron cloud, the electron cloud is pulled away from the nucleus and the displacement creates an atomic dipole [8]. Blue represents negative charge and red denotes positive charge.

Since the electric field oscillates, the created atomic dipole will also oscillate. The probability of an excitation of the atom is high if the oscillation of the field is similar to an intrinsic oscillation mode of the atom, but if it is not, the oscillation is unlikely to be sustained by the atom after the field has passed and thus stopped driving the motion. In other words, if the oscillation frequency of the incident light is not close to an intrinsic frequency mode of the atom, no excitation is likely to occur [9]. While the field and the atom interact, they form a shared system with a shared energy; if an excitation occurs, the energy required for the sustained oscillation will originate from this shared energy. This means that if an excitation occurs, the field leaves the interaction with less energy than it had before the interaction, while the atom has gained energy from the interaction and may oscillate for some time after the field has passed. Nevertheless, the atom acts as an oscillating dipole and must therefore radiate, which causes a loss of energy and therefore the amplitude of the oscillation must decay [10].

The decay of the atomic dipole oscillation is inherently exponential, which means that the intensity will decay as $I = I_0 \exp(-t/\tau)$, where I_0 is the intensity at the excitation moment, and τ is the decay time of the state. The decay time is generally shorter than the natural lifetime of the state [11]. The decay time and its pressure dependence are important characteristics for the method that this thesis evaluates.

The radiated field from the atomic oscillating dipole will interfere with the incident field, and the total field will therefore be dependent on whether there is a phase shift or not between the incident field and the radiated field. To find the phase shift it is necessary to go into some mathematical descriptions. First the induced oscillations of the electron cloud need to be described, then from the expression for the electron cloud position it is possible to find the expression for the radiated field from the atomic dipole. It is sufficient to treat the electron cloud oscillation since the nucleus is heavy compared to the electrons and therefore it will be mainly the electrons that shift their position.

First, the position of the electron cloud is found by approximating the atom to be a harmonic oscillator, such that its motion is given by

$$m\left(\frac{d^2x(t)}{dt^2} + \omega_e^2 x(t)\right) = F_d, \tag{1}$$

where m is the mass of the electron, $x(t)$ is the displacement at a time t from the equilibrium position where the center of the electron cloud and the nucleus coincide, ω_e is the natural frequency of the electron movement and F_d is the force driving the motion [10]. However, the situation applicable for this project is one where the atoms are excited by the incident field to a higher state than their ground state, which means that there is a non-zero probability of them decaying to a lower energy state and therefore the amplitude of the oscillation must be damped. If the damping is taken into consideration, Eq. 1 should be rewritten into

$$m\left(\frac{d^2x(t)}{dt^2} + \gamma\frac{dx(t)}{dt} + \omega_e^2 x(t)\right) = F_d, \tag{2}$$

where γ is the damping coefficient. The next step needed to find the phase shift between the incident field and the radiated field is to find the driving force, which is given by the incident electric field multiplied by the charge of the electron, so Eq. 2 can be rewritten into

$$m\left(\frac{d^2x(t)}{dt^2} + \gamma\frac{dx(t)}{dt} + \omega_e^2 x(t)\right) = q_e E_0 e^{i\omega_i t}, \tag{3}$$

where q_e is the charge of the electron, E_0 is the amplitude of the incident field, and ω_i is the frequency of the incident field [10]. Eq. 3 is a differential equation with the solution

$$x(t) = \frac{q_e E_0}{m\left(\omega_e^2 - \omega_i^2 + i\gamma\omega_i t\right)} e^{i\omega_i t}. \tag{4}$$

Eq. 4 is true for all electrons of the atom, although the zero point of the oscillation may be different for each electron [10]. This means that the radiated field from the

electrons can be treated as a sheet of oscillating charges, all moving together. The electron sheet approximation is sufficient because it is only the motion perpendicular to the propagation direction of the light that creates a field in the propagation direction [10]. The field created by such a sheet of moving charges can be expressed as:

$$E_a(z,t) = -\frac{\eta q_e}{2\epsilon_0 c} v(t - z/c) \tag{5}$$

where E_a is the field created by the electrons at a distance z from the electrons along the propagation direction of the light, ϵ_0 is the vacuum permittivity, η is the number of charges per unit area, and $v(t - z/c)$ is the velocity of the electrons parallel to the sheet at a time $t - z/c$ [10]. To find the velocity, Eq. 4 is differentiated at $t = t - z/c$. The velocity is then inserted into Eq. 5 to find the final expression for the field created by the atomic dipole [10]:

$$E_a(z,t) = -\frac{\eta q_e}{2\epsilon_0 c} i\omega_i \frac{q_e E_0}{m\left(\omega_e^2 - \omega_i^2 + i\gamma\omega_i\right)} e^{i\omega_i t}. \tag{6}$$

What should be especially highlighted from Eq. 6 is that if $\omega_i \approx \omega_e$, Eq. 6 can be rewritten into:

$$E_a(z,t) = -\frac{\eta q_e}{2\epsilon_0 c} i\omega_i \frac{q_e}{mi\gamma\omega_i} E_0 e^{i\omega_i t} \tag{7}$$

$$E_a(z,t) = -\frac{\eta q_e^2}{2\epsilon_0 c m\gamma} E_0 e^{i\omega_i t} \tag{8}$$

where it can be seen that the interaction of the radiation with the atomic dipole creates a field that is anti-parallel and proportional to the incident field. This results in a destructive superposition and therefore to a dampening of the incident field. This is the phenomenon that gives the extinction of light for certain frequencies in an absorption spectrum; these certain frequencies coincide with an intrinsic frequency of the material and the interference is therefore destructive in accordance with Eq. 7.

However, the standard process of light-matter interaction described above can be modified. This is because the energy levels of an atom are shifted to a higher or lower energy when the atom is perturbed by a non-resonant electric field [11]. Usually, the temporal evolution of the phase of the oscillating dipole is given by:

$$\phi = \frac{E \cdot t}{\hbar} \tag{9}$$

where ϕ is the phase, E is the energy of the state, t is the time that has passed since the excitation and $\hbar$, as usual, denotes the reduced Planck's constant. However, when the energy is shifted by an external field, the expression for the phase changes into:

$$\phi + \Delta\phi = \frac{E \cdot t}{\hbar} + \frac{\Delta E \cdot t}{\hbar} \tag{10}$$

where $\Delta\phi$ denotes a small phase shift. ΔE, the small energy shift, in turn depends on the intensity of the electric field such that if the intensity increases, the magnitude of ΔE also increases. This means that a larger intensity of the perturbing field gives a larger phase shift of the atomic dipole [12].

2.2 Macroscopic effects

The discussion above concerns atoms in an electric field where the atoms are unaffected by the dipole response of adjacent atoms; this section will discuss what happens when the effect of adjacent dipole responses is significant.

2.2.1 Steering through phase control

A macroscopic effect that is important to this thesis project is what happens when the radiation fields from different decaying dipoles with different phases are superposed onto each other; this phenomenon actually allows for steering of the radiated light. To understand this, one may look to another field of physics: radar technology. Radar technology has for a long time used phase changes to steer array radars. The technique is based on the fact that in a linear medium, such as air or vacuum, the direction of the energy of the radiation is perpendicular to the wave front [13] as seen in Fig. 2.

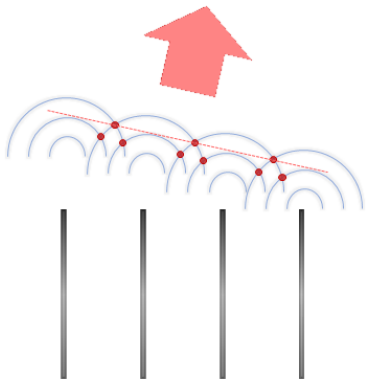

Figure 2: Schematic illustration of how a phase change is used to steer radiation in an array radar. The red circles marks where there is constructive interference of wave crests, and the red arrow where the total radiation is directed.

Redirection of the wave front can be obtained by tailoring the phase of each antenna, i.e. the timing when an individual antenna emits a wave front is manipulated. This means that a phase gradient across a row of antennas can be created, as depicted in Fig. 2. This leads to a shift in the direction of the emitted radiation, because it is only in the new direction that there will be constructive interference between the signals from all antennas [14] as seen in Fig. 2. All other directions will be suppressed by destructive interference [14]. These interference and redirection effects are only possible if the radiation was coherent to begin with, otherwise the phase of the light would not be possible to manipulate into a phase gradient and the interference effects would not enhance one direction and suppress other directions in the same way.

This principle of obtaining spatial control by using phase control has recently been proven to enable steering of coherent XUV light, see [7]. The phase gradient is in that case introduced by using a non-resonant laser pulse, which inflicts a shift in the phase of excited, radiating atoms (given by Eq. 10). This means that the direction of the total radiated light can be modified, since the ability to modulate the phase automatically gives the ability to modulate the direction of the total radiated

light, as previously mentioned (Sec. 2.2.1). This technique was used for this project and will therefore reappear in the Method section (Sec. 3).

2.2.2 Resonant pulse propagation

If the concentration of atoms in the studied system is high, the single dipole response picture is not a physically reasonable approximation for the whole system. For example, one thing that can occur in dense gases is resonant pulse propagation (RPP), which happens when the states that the atoms are excited to are long-lived compared to the pulse duration, and the amplitude of their dipole response is large enough to significantly alter the field that is incident on atoms after them [15].

RPP can be seen in emission spectra as an oscillatory modulation in the exponentially decaying structure that comes from the single dipole response. For the case of a resonant field, RPP can be explained with Fig. 3. Fig. 3 is obtained from a simulation of how an incident Gaussian pulse interacts with a second field that is proportional to the intensity of the first pulse but π radians out of phase to it. The black line shows the absolute value of the total amplitude when these two fields interfere. This simulates the first step of the RPP process: the first modulation minimum appears due to a superposition of the incident field and the secondary field that is created by all the atomic dipoles. Since the incident field is resonant with the transition, the secondary field is out of phase with the first field [16], as seen in the opposite signs of the red and blue amplitudes in Fig. 3. This means that the incident field and the secondary field will interfere destructively. It can also be seen that there is a local maximum when the pulse has passed but the exponential decay of the atomic dipole response has not diminished significantly yet. This shows why RPP is only present for pulses where the duration is short compared to the decay time of the excited state.

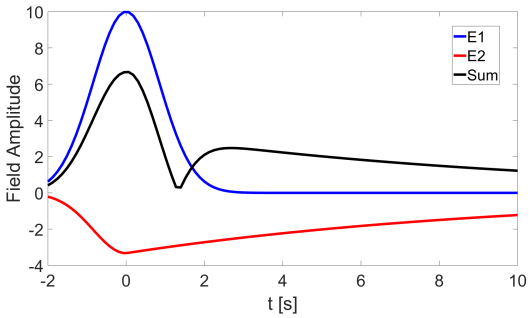

Figure 3: The result of a simulation where a Gaussian pulse interacts with a field that is proportional to the Gaussian pulse but has the opposite sign and decays exponentially. The decay time for the exponentially decaying field was for this result set to 5 seconds, and the σ-parameter of the Gaussian was set to 0.6 s. The black line denotes the absolute value of the sum of the blue and the red field amplitudes.

However, this simplified picture is just the first step of the RPP-process and is not sufficient for real situations but must be expanded. In reality, the field marked with black in Fig. 3 will serve as the incident field for interactions with atoms further along in the path, and their atomic dipoles will create a third field that is out of phase with the second field, so that another minimum followed by a maximum is created, and so on [16]. However, since some of the radiation of the second field

was sent out during the time the initial pulse was still present, the amplitude of the second local maximum will not be as high as the amplitude of the initial pulse, as seen in Fig. 3. The same reasoning applies to the following fields, so that the amplitude will decrease for each local maximum [16].

It is worth mentioning that RPP is present even for cases when the total phase shift is not π. For example, the second field could instead be in phase with the first field, which is also in phase with the third and all succeeding fields. This is the case when some auto-ionizing states, that is, states above the ionization threshold, interact with light. Auto-ionizing states are characterized by that there are two paths for the atom to end up in the same energy state: either by absorption to the discrete state or by ionization into the continuum of energy of a free electron. These two possibilities will cause a quantum interference effect [12]. This may sound strange, but according to quantum mechanical theory the position of a particle is given by a probability wave; and due to this wave characteristic, quantum path interference can and does occur. Quantum path interference affects the excitation process for auto-ionizing states, such that the phase is shifted. For some auto-ionizing states, the additional phase shift due to quantum path interference cancels out the ordinary phase shift given by Eq. 6, and these states are called window resonances [12].

The macroscopic phenomena that have been discussed in this report are not by any means the only important macroscopic phenomena that affect the atomic dipole decay. No other phenomena will be discussed in detail, but there are multiple effects that can change the decay time and structure, as well as change the phase. An example of another effect is the free induction decay, where it is the coherence between the different radiating dipoles that decays, which results in the total field decaying faster than the individual decay time for the atomic dipoles [17].

A common characteristic for the effects that affect the decay time is that they grow stronger as the pressure grows higher, since a higher pressure gives smaller spacing between the atoms and thus the dipole response fields end up closer to each other and can affect each other stronger. Of course, a higher pressure could also mean that there are more atoms that can give a dipole response to the field.

3 Method

The evaluation of the proposed method was done by performing decay time measurements following the procedure outlined in the method scheme given in Sec. 3.1, and then analyzing the data to make sure the results were consistent over time. The effects of changing the pressure as well as the effects of changing other parameters were evaluated to see whether any macroscopic effects could be distinguished from the results. The results were also compared to previous lifetime measurements of the same states [18], to see if the decay time seems to be approximately the natural lifetime or if other effects are present in the setup.

3.1 Proposed method scheme

The principle behind the proposed method follows from a way of controlling light using light [5][7] as described in Sec 2.2.1. In short, coherent XUV-light is sent

through a noble gas target, where the XUV-light excites the atoms. Thereafter an ultrashort IR-pulse is used to modulate the phase of the decaying atoms, which creates a deviation from the original beam path. The deviation is used to separate the signal and the transmitted XUV-light, thus obtaining a higher signal-to-noise ratio, SNR, than what was previously possible [18].

The method should also be able to provide a precise time resolution. This is due to the fact that it is the time delay between two pulses that gives the time resolution, and the time delay can be adjusted with high precision.

This higher SNR and good time resolution should lead to a high precision in the determination of the decay time of the evaluated state, and hopefully enable identification of which decay processes are present. The decay processes should be possible to identify by their pressure dependence, thus the measurement is repeated for different target gas pressures to check which effect the gas pressure change inflicts on the decay time. Identification of the decay processes requires a precise measurement as there are several different macroscopic processes that depend on the intensity of the incoming light and the pressure in different ways [17], which means that the fitting process requires the use of many variables. The more variables a fitting needs to take into account, the more precision is needed in the data to obtain trustworthy results. With this in mind, it is not difficult to see why the macroscopic processes in a decay process have evaded precise characterization [1].

The characterization of decay processes is not only interesting for fundamental research, but could also be used as a calibration for the intensity of the redirected light in the developing OOM technique that was mentioned in the introduction (Sec. 1) and in the theory (Sec. 2.2.1). This intensity calibration would be performed by adjusting the timing between the initial excitation and the redirecting, phase-modulating probe pulse so that the redirection occurs when exactly the desired fraction of the intensity remains and the excess has been radiated away before the probe pulse. Perhaps it would also be possible to use a second phase-modulating pulse to redirect the light back onto the first path, and then the delay between the two modulating pulses could be used to further tailor the intensity of the pulse.

The states that were chosen for evaluation are states that are deemed suitable for redirection, that is, states that are clearly separated in energy from other states. The separation is necessary to avoid intensity fluctuations due to population oscillations between the neighboring states [19], which would add yet another process that affects the decay time and the intensity available for redirection at a certain time delay between the excitation pulse and the redirecting pulse.

The data presented in this thesis was sampled in January, February and March of 2018.

3.2 Setup

The experiment was performed using an existing setup, namely the one used in [7]. An overview is given in Fig. 4. The laser is a Ti:sapphire laser system centered at a wavelength of 800 nm, which has a repetition rate of 1 kHz. The pulse length of the pulses obtained from the laser system is 20-30 fs. The laser pulse creation, amplification and shaping have not been the focus of this experiment, so they will not be discussed further in this thesis; the process is described in detail in [20].

The next step in the setup is the area where the beam is split and daily align-

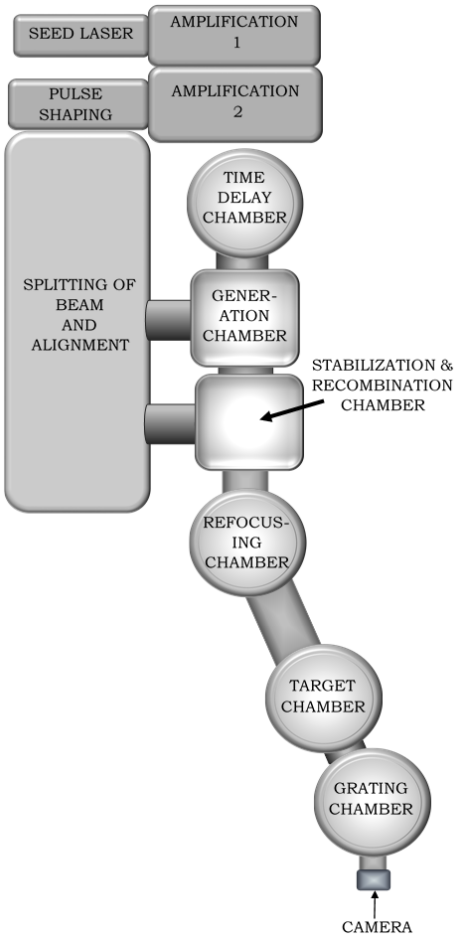

Figure 4: Schematic overview of the setup used for the experiment.

ment is performed using a He-Ne laser, which is later also used for stabilization [5]. The He-Ne laser is stable and aligned to be coaxial with the IR beam that is produced in the first steps, so that the stabilization and alignment can be performed using the He-Ne beam as a stable reference.

The beam is split in this step by sending it through a mirror with a spherical hole. The reflected part forms the pump beam, which thus becomes annular, and the transmitted part is used as a probe beam. The beams are sent through optical components in such a way that they propagate separated but parallel into the first vacuum chamber [5] as illustrated in Fig. 5. Mirrors placed on remotely controlled translation stages are used to create a difference in path length between the two beam paths, which enables an adjustable time delay between the pump pulse and the probe pulse. This description is a simplification that excludes a discussion about the holey mirrors and focusing necessary to enable the main path shown in Fig. 5; for a discussion of these details, see [5].

During a measurement, the mirror mounted on a translation stage belonging to the path of the probe beam (blue in Fig. 5) is moved to change the time delay between the pulses. The translation stage has enough precision that the smallest delay step needed for this project, 5 fs or equivalently 1.5 μm difference in path length, could be obtained.

After the pump beam has passed the time delay chamber, it reaches the gas jet.

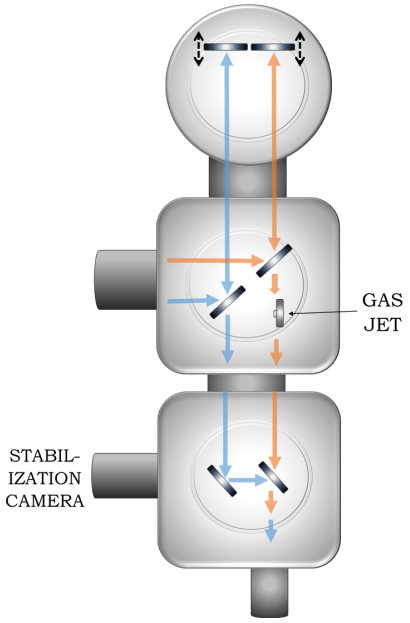

Figure 5: Schematic overview of the vacuum chambers denoted generation chamber, time delay chamber and stabilization & recombination chamber in Fig. 4. The figure depicts translation stages and mirrors that are needed to impose a time delay between the two paths, as well as the gas jet supplying the gas needed for High-order Harmonic Generation.

In the gas jet, XUV-light is created using HHG, the technique that was mentioned briefly in Sec. 1. HHG is a process where non-linear light-matter interaction is utilized to produce odd harmonics of the driving frequency of the incoming laser light [3][4]. There is a research field in itself around HHG, and the process has not been the focus of this thesis, therefore the reader is directed to [21] for an in-depth account of HHG at Lund University.

The gas jet used both to provide Argon atoms for the HHG process and to the target gas is a pulsed-valve GR020 from Attotech. The opening of the pulsed valve is controlled by a piezo crystal, which in turn is controlled by an external voltage [22]. This means that the higher the applied voltage, the larger the opening and the more gas is let out into the vacuum chamber. The GR020 supports backing pressures, that is, the pressure that is built up behind the valve, up to 5 bars [22]. This pulsed valve technique enables experiments with high gas pressures while keeping the ambient pressure low.

The XUV light emitted from the HHG continues on the path marked with orange in Fig. 5 into the stabilization and recombination chamber. The stabilization of the delay between the pump and the probe utilizes a number of remotely controlled optical instruments, a camera, and the He-Ne beam. Since the He-Ne beam co-propagates with the IR-beam at the splitting point, parts of the He-Ne beam co-propagates with the pump and then with the XUV light, while the rest of the He-Ne co-propagates with the probe [5]. The camera detects the drift of the different path lengths by comparing the phase of the He-Ne beams travelling the different paths, and then an automated system compensates the drift by adjusting remotely controlled optical instruments [5]. The stability of the laser system after the recombination of the beams is ± 0.1 fs. The focus of this project has not been

on the stabilization process, therefore it will not be discussed further. Additional information on the stabilization process can be found in [5] and [20].

One final detail about this chamber that is of importance to this thesis is that before the light leaves the stabilization and recombination chamber, it passes through an aperture and then recombines with the probe by the use of another holey mirror. Since the IR beam that is used in the HHG process (the pump) is the part of the beam that is reflected by the first holey mirror, the IR beam is annular; this means that the passage through the aperture removes most of the IR light that remains after the HHG process. However, it also affects the harmonics used in the experiment in that their spatial extent becomes limited [20].

After the stabilization and recombination chamber, the pulses continue on into the refocusing chamber, where a toroidal mirror is used to refocus the beam that now contains both the XUV pump and the IR probe. The mirror focuses the mixed beam into a second gas jet, located in the target chamber [20], as illustrated in Fig. 6.

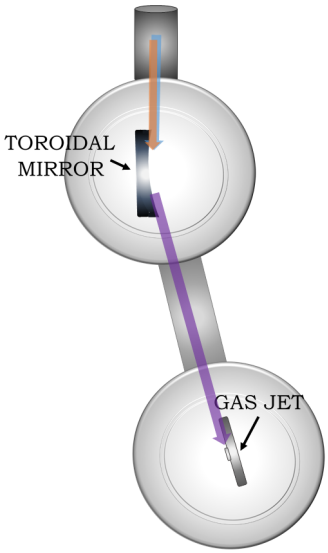

Figure 6: Schematic overview of the vacuum chambers denoted refocusing chamber and target chamber in Fig. 4, where the mixed beam that is obtained from the stabilization and recombination chamber is refocused. The toroidal mirror is adjusted so that the focus is in the tube of the gas jet in the target chamber.

In the target chamber, the XUV pump and the IR probe interact with atoms emitted from the second gas jet, as illustrated in Fig. 8. As previously mentioned, the gas jet is identical to that used for the HHG-process (GR020 from Attotech). The tube where the gas flows and interacts with the beam at its focus has a diameter of about 1 mm. Before the experiments were performed the gas jet in the target chamber was temporarily removed from the setup, and a sharp edge mounted on a translation stage was inserted in its place to evaluate the beam spot size in the target gas. The measurement was performed by moving the edge horizontally and comparing the transmitted intensity for different positions, and then the procedure was repeated for the vertical direction. The beam spot size was then found by assuming a Gaussian beam shape and fitting a cumulative Gaussian distribution to the data.

The interaction in the gas jet tube begins when the XUV-light excites the atoms ejected from the jet, then the atoms decay during the time delay between the XUV-light and the probe pulse. The light that is emitted during this time continues on the same path as the XUV-light that excited them. Once the probe pulse reaches the target gas jet, it inflicts a phase gradient over the atoms. This phase gradient follows from the fact that there is an intensity gradient from the center to the edge of the probe, according to Eq. 10. This phase gradient creates a redirection of the emitted radiation as follows from Sec. 2.2.1, which separates the emission of the atoms from the light that is transmitted through the gas without interacting with the atoms. The transmitted light becomes the on-axis radiation in Fig. 7, while the light that is emitted from the decaying atoms after the interaction with the probe will be shifted up or down - in the example presented in Fig. 7 the emission is redirected upwards.

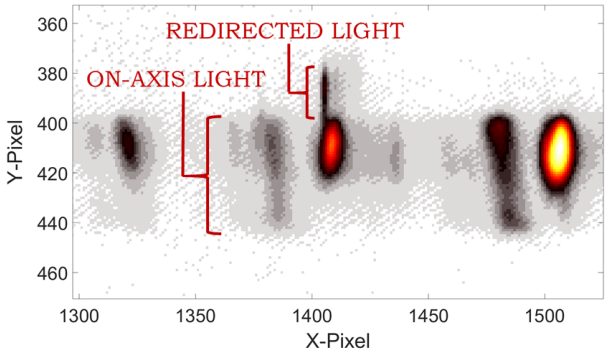

Figure 7: Example of a spectrometer image showing redirected as well as transmitted light; the transmitted light is the on-axis radiation while the redirected light for this case was directed above the on-axis light.

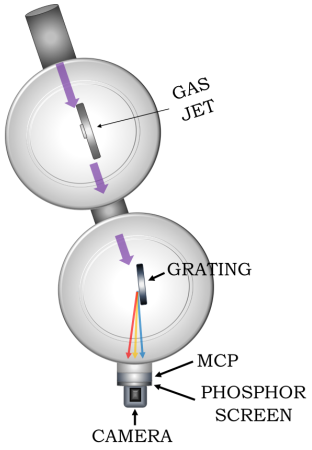

Figure 8: Schematic overview of the vacuum chambers denoted target chamber and grating chamber in Fig. 4. The light from the gas, both the emission and the light that is only transmitted, is split into its frequency components by a reflection grating. After the grating, the light is detected by a microchannel plate (MCP) and a phosphor screen, which is imaged by a camera.

The next step in the setup is a focusing XUV reflection grating (Hitachi grating

001-0639), where both the redirected light and the on-axis light is separated into its different frequency components [5]. The light from this, and any generic grating, will give rise to several diffraction orders (q) that can sometimes create confusion in the analysis of the output. The deflection angle ($\Delta\theta$) inflicted by the grating can be calculated as:

$$\Delta\theta = q \cdot \frac{c}{\nu\Lambda} \tag{11}$$

where ν is the frequency and Λ is the line spacing of the grating [13]. Assuming that $\Delta\theta$ is small enables the use of the paraxial approximation to find the deviation from the original path (Δx) after a distance d:

$$\Delta x = d \cdot q \cdot \frac{c}{\nu\Lambda}. \tag{12}$$

For this experiment, it is assumed only the first and second diffraction order will be visible on the screen. The distance on the screen between two harmonics for the first order (Δx_{odd_h}) can be found by using that the frequency difference between two odd harmonics is twice the fundamental frequency ν_0:

$$\Delta x_{odd_h} = d\frac{c}{\nu_0 \cdot \Lambda} - d\frac{c}{\nu_0 \cdot 2\Lambda} \quad \Leftrightarrow \tag{13}$$

$$\Delta x_{odd_h} = d\frac{c}{\nu_0 \cdot 2\Lambda}, \tag{14}$$

where the lower harmonic for simplicity is chosen to be the first. For the second order, however, the distance between two odd harmonics is given by

$$\Delta x_{odd_h} = 2 \cdot d\frac{c}{\nu_0 \cdot \Lambda} - 2 \cdot d\frac{c}{\nu_0 \cdot 2\Lambda} \quad \Leftrightarrow \tag{15}$$

$$\Delta x_{odd_h} = d\frac{c}{\nu_0 \cdot \Lambda}, \tag{16}$$

where the lower harmonic once again is chosen to be the first. Even if the paraxial approximation might not be completely justified for this setup, the approximate distance between the harmonics can still be used to indicate which order is being imaged.

Since the frequency analysis is performed using a grating with vertical slits, no horizontal deviation can be detected and thus the probe beam should be adjusted such that it only modulates the phase vertically; any potential horizontal deviation could be misinterpreted in the analysis of the emission spectrum as light that is of a different frequency.

The frequency separated light is then finally detected by a microchannel plate (MCP) connected to a phosphor screen (Photonis) and imaged by a charge-coupled device (CCD) camera (Pike F-505B from Allied Vision Technologies) [5].

A final detail that needs to be discussed about the setup is that there are pressure gauges connected to the generation and target chambers. These pressure gauges measure the ambient pressure in each chamber. Since the vacuum chambers are continuously drained of particles by turbomolecular pumps [5], the ambient pressure is mainly dependent on how many particles are injected by the gas

jet; in this way, the amount of generation or target atoms is monitored and possible to adjust. However, it should be emphasized that the measured pressure is not the actual pressure in the gas jet itself.

3.3 Data processing and fitting

A couple of different methods of data processing were evaluated in the project and will be discussed. The first step for all of them is to remove the background noise. This is done by taking a background image with the camera when both beam paths are blocked, and then subtracting the measured background intensity from each pixel for the snapshots taken during the time delay scan. An example of the resulting image is shown in Fig. 9. To obtain a measure of the decay, the pixels in the area corresponding to the redirected light are singled out and the measured intensities of the pixels are integrated. This intensity sum is then stored for each frame, which corresponds to each time delay point. Looking at the intensity sums over time gives a result like the one in Fig. 10.

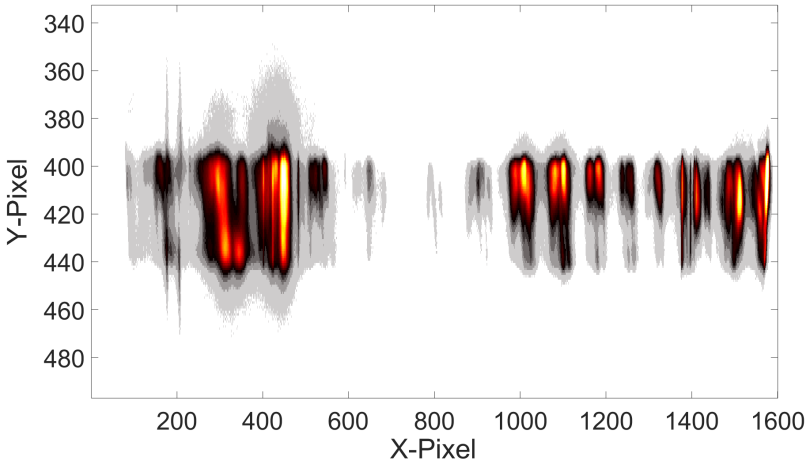

Figure 9: Example of a spectrometer image after the background noise has been removed. This particular scan is taken with Argon as target gas.

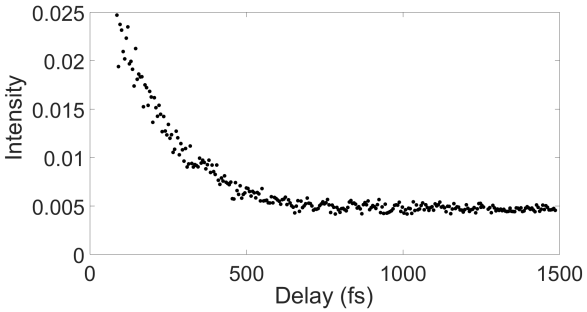

Figure 10: Example of the resulting plot after the pixel intensity of the area with redirected light has been integrated for each time delay measurement. This particular scan was taken in Neon, with an ambient pressure of $3.0 \cdot 10^{-5}$ mbar in the target chamber.

After the intensity sum is obtained, the different methods start to diverge. One option is to simply fit a function to the intensity sum as it is, or normalizing it first.

A second option is to correct for any possible deviation between the requested delay value and the actual delay caused by the translation of the mirror in Fig. 5. This correction is made with the aid of a function that is built into the stabilization software: the software can log the position of the moving mirror and plot it against the position request from the scan. An example of such a plot is shown in Fig. 11. The measured intensity is then assigned to the actual delay, marked with an unbroken blue line in Fig. 11.

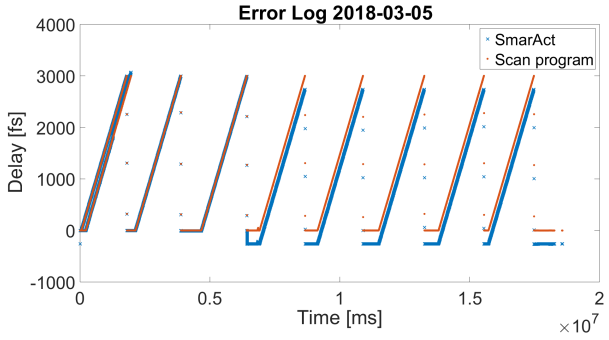

Figure 11: Example of an error log extracted from the laser stabilization program. The red dots marks the time delay requested by the scanning software and the blue crosses marks the actual time delay calculated from the position of the SmarAct translation stage holding the mirror.

After the delay correction, the laser fluctuations are analyzed. A few different methods of compensating for the effect of the laser fluctuations were evaluated. The first one uses the on-axis radiation to measure the fluctuations, and assumes a linear scaling between the on-axis intensity and the redirected light. This assumption is based on the idea that the intensity fluctuations of both the transmitted light and the redirected light should originate in the intensity fluctuations of the incident laser pulse. This linearity is then used to compensate for fluctuations by dividing the redirected intensity by the on-axis intensity. Note that in this reasoning the light of the harmonic resonant with the transition is not included in the on-axis intensity since it should be diminished when light is redirected.

A second method of laser fluctuation compensation is based on the idea that if the laser power did not fluctuate, the sum of the intensity of the harmonic overlapping with the evaluated state and the redirected light should always be constant. This means that rather than looking at the measured intensity as is, instead the fraction of the total intensity that has been redirected is monitored. This would ideally make the method insensitive to laser fluctuations. It should be emphasized that this is only an approximation, since the probe intensity also will fluctuate and thus ionize a different amount of atoms in the gas, and the ionized atoms do not contribute to either the intensity of the resonant harmonic or the redirected emission. However, the intensity of the probe is proportional to the intensity from the laser, while the non-linearity of the HHG-process makes the laser fluctuation dependence of the XUV-light difficult to predict. This means that it is possible that the XUV-light experiences much larger fluctuations than the probe, which would mean that the approximation of a constant intensity over the resonant harmonic and the redirected emission is justified.

The third method to reduce fluctuation impact that was evaluated investigates the correlation between the on-axis intensity, except for the resonant harmonic,

and the redirected light. Ideally, the correlation should be zero and any correlation that occurred would then be caused by laser fluctuations. Thus, it should be possible to compensate for the laser fluctuations by finding the relation that gives the least correlation between the on-axis intensity and the redirected intensity. This was done by evaluating different relations between the two intensities with optimization routines. The relation that gives the minimum correlation was used to compensate for the intensity fluctuations by division of the redirected intensity by first a first order polynomial of the on-axis intensity and then a second order polynomial, where the polynomial is optimized with respect to the correlation function between the two intensities. The resulting signal can then be analyzed as is and should ideally not contain any correlation to the laser fluctuations.

Finally, a deconvolution method to reduce the effect of the laser fluctuations was evaluated briefly. The reasoning behind this approach also utilizes the on-axis intensity as a measure of the laser fluctuations, which are then regarded as a known noise pattern in the redirected intensity. Known noise patterns can sometimes be removed using deconvolution [23]. To perform the deconvolution between the redirected light and the on-axis intensity, both the built-in MATLAB function *DECONV()* and a code written especially for this project was evaluated.

The data fitting was performed using a least-squares method, where an exponentially decaying function was fitted to the experimental data. The exponentially decaying function is given by the following expression:

$$I = C_1 \cdot e^{-\tau^{-1}(t-C_2)} + C_3 \tag{17}$$

where I is the intensity at a delay of t seconds, τ is the decay time of the state, C_1 is a scaling coefficient, C_2 is a coefficient giving the time for the start of the decay, and C_3 is a coefficient describing any background remaining despite the background subtraction. The built-in MATLAB function *FMINSEARCH* was used to find the minimum sum of squared residuals between the exponential decay of Eq. 17 and the experimental data, using a guess for the best coefficients and the redirected intensity as input.

In order to check the stability of the method, several delay scans with the same parameters were taken back-to-back on most occasions, so that a couple of ideally identical scans formed a set. The decay times extracted from individual fits to these duplicate scans were compared to the decay time that was extracted when the fitting was expanded so that all scans in the set were taken into account. This expanded fitting allowed C_1, C_2 and C_3 to vary from scan to scan while the decay time was forced to be identical for the entire set. Several sets of scans were taken for each pressure value to check for any pressure-induced changes in the decay time as well as checking the stability of the method from day-to-day.

The quality of the results was also evaluated by looking at a few different correlations. This could be for example evaluation of the gas pressure fluctuations caused by the gas jet, which can be deduced by comparing the correlation between the intensity of the frequencies that should be affected by the gas, namely those energetic enough to ionize the gas, compared to the frequencies that should not be affected by the gas.

The evaluated states were identified by comparing the frequency distance between the odd harmonics to known reference lines [24][25][26] to find the effective fundamental frequency for the harmonics. This may differ from the given

frequency of the driving laser due to a non-linear process known as ionization-induced blue-shifting [27]. The blue-shifting is a phenomenon that occurs when the intensity of a pulse is high enough to ionize gas atoms into a plasma, which leads to a spectral broadening of the pulse. The intensity of the higher frequency components is then enhanced, which leads to a higher central frequency of the pulse [27]. Once the effective fundamental frequency is known, the odd harmonics can be used in addition to the known reference lines to perform a calibration of the horizontal pixels of the CCD camera into frequency, which allows the atomic lines to be identified.

4 Results

In this section, the results from the thesis project will be presented. Before analyzing the delay scans and the possible correlations between different error sources, identification of the lines will be discussed. But first, the results of the beam spot size evaluation will be briefly discussed.

4.1 Target beam spot size evaluation

The beam spot size in the target gas was evaluated by moving a sharp edge and then fitting a cumulative function to the transmitted intensity, as described in the method section (Sec. 3.2). Some examples of scans and corresponding fitted cumulative distribution functions are given in Fig. 12. For this particular position along the optical axis (z-position), the scans indicate a horizontal FWHM of about 50 μm and a vertical FWHM of about 62 μm.

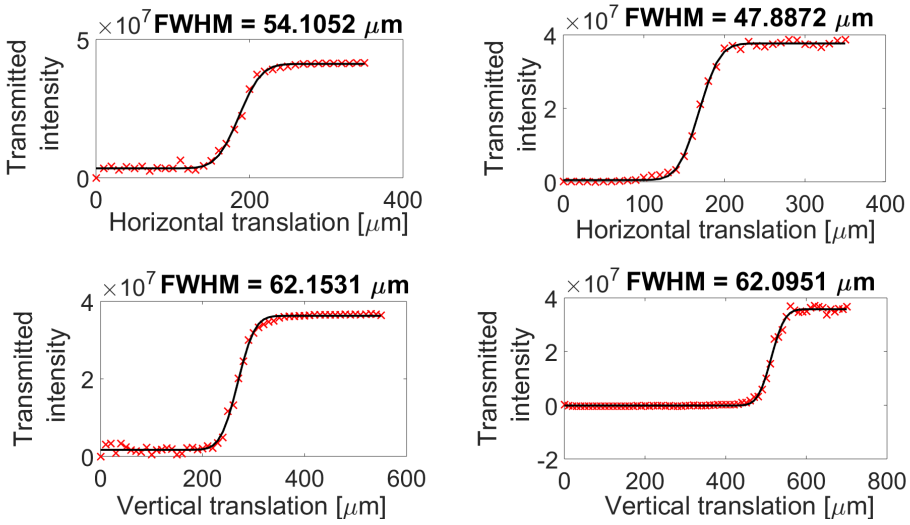

Figure 12: Beam spot size measurements, where the distance from the maximum to half the maximum intensity indicates half of the FWHM of the beam spot. The measurements were performed twice, with a change of starting point between the measurements. This was done to prevent any hysteresis effects of the translation stages used in the measurements. Red crosses marks the experimentally obtained transmitted intensity and the black line shows the fitted cumulative distribution with a full-width at half-maximum (FWHM) as indicated in the figure.

However, the values for the FWHM were changing depending on the z-position. For example, for another z-position the horizontal FWHM was found to be about 160 μm and the vertical FWHM was about 37-38 μm, while for yet another z-position the horizontal FWHM was about 30 μm and the vertical about 160 μm. These large beam spot size differences were obtained for a difference in the z-position of 0.5 cm. This indicates an astigmatic beam and it also indicates a shorter focus and de-focusing region than expected. From the shorter focus region follows that the sensitivity of the placement of the target gas jet was higher than anticipated.

4.2 Identification of the emission lines

A camera image from the 20^{th} of February was used to identify the emission lines in Argon that were studied; the image and reference lines [24][25][26] are shown in Fig. 13.

The reference lines were used to fit a calibration curve to the spectrum. The odd harmonics seen in Fig. 13 could then be identified and the fundamental frequency adjusted for the effect of blue-shifting. However, even after shifting the fundamental frequency the harmonic spectrum did not seem to fit with the reference lines as shown in Fig. 14. The distance between the odd harmonics seems closer to one driving frequency than to two, which would be the case if the harmonics used for the calibration are in fact from the second diffraction order of the grating, as given by Eq:s 13 and 15. This scenario was evaluated in Fig. 14b, and as can be seen from the figure this coincides better with the reference lines.

Assuming the harmonics belong to the second order, the calibration curve coincides well both with the reference lines and the harmonics and can thus be used to rescale the spectrometer images to show the energy scale instead of X-pixel scale on the x-axis. The result is shown in Fig. 15.

The emission lines that were studied in Argon have a higher energy than the ionization threshold; this conclusion is drawn due to the fact that the decrease in intensity of the harmonics, that is due to the strong absorption near the ionization threshold, appears to the left of the emission lines in Fig. 15. This indicates that the emission lines belong to the auto-ionizing states in Argon. A couple of candidates as to which states the emission lines could belong to are given in Tab. 1; from the table and Fig. 15, it can be seen that the left emission line probably belongs to $3s3p^6 7p$, while the right emission line probably belongs to $3s3p^6 8p$.

Table 1: Auto-ionizing states in Argon [24][25][26].

Configuration	Emission line [eV]
$3s3p^6 9p$	28.99
$3s3p^6 8p$	28.90
$3s3p^6 7p$	28.76
$3s3p^6 6p$	28.51
$3s3p^6 5p$	28.00
$3s3p^6 4p$	26.62

Looking at previously recorded measurements of $3s3p^6 7p$ and $3s3p^6 8p$ [18], it is stated that the authors found an energy broadening of 6.6 ± 0.5 meV for $3s3p^6 7p$,

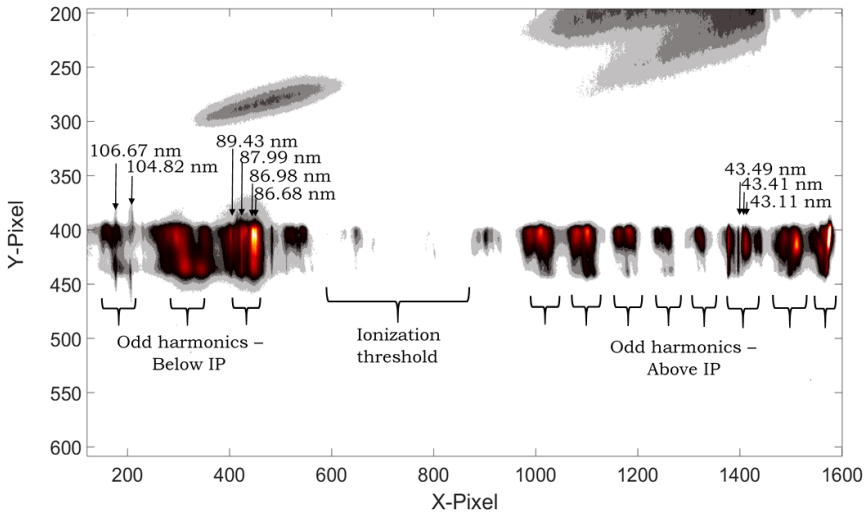

(a)

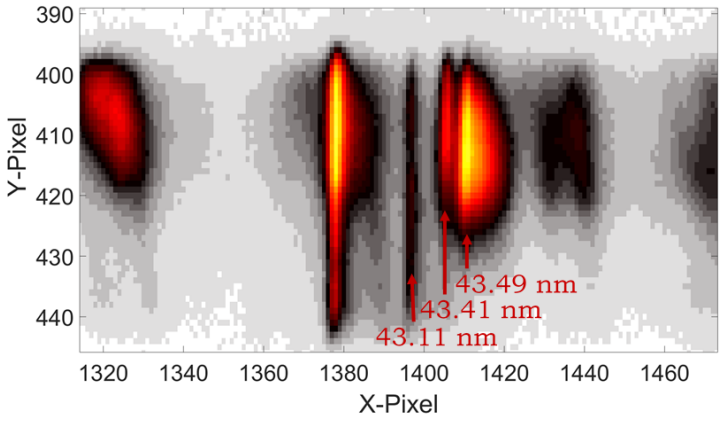

(b)

Figure 13: Spectrometer image with marked reference lines that were used to identify the evaluated states in Argon. Only the odd harmonics are created in the High-order Harmonic Generation technique, thus the spectrum only consists of the atomic lines and the odd harmonics. The ionization potential (IP) can be deduced from the suddenly reduced intensity of the harmonics.

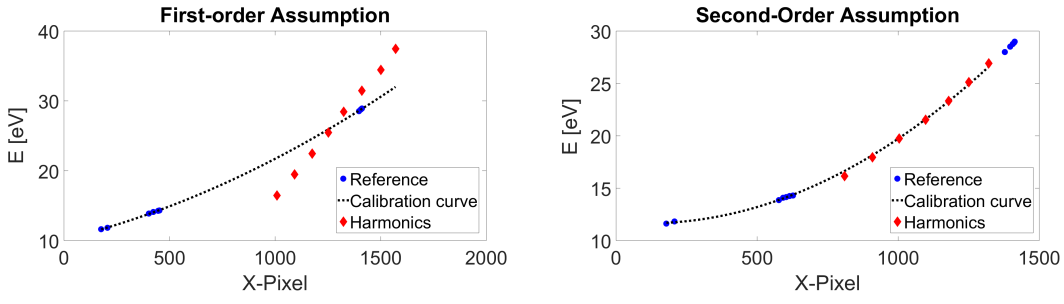

(a) **(b)**

Figure 14: Comparison between the assumptions a) that the odd harmonics seen as on-axis radiation in Fig. 13 belong to the first order, and b) that the odd harmonics belong to the second order.

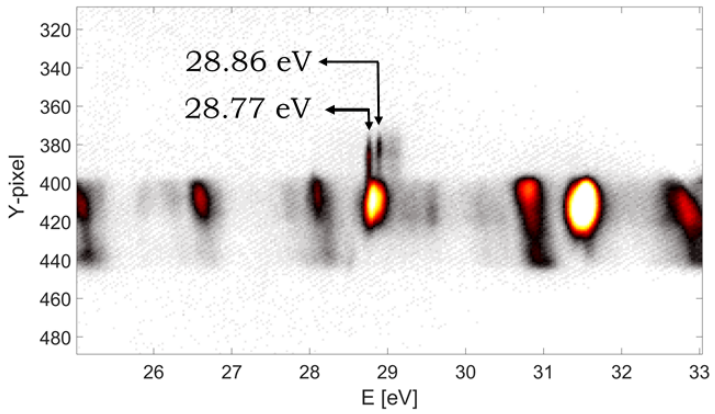

Figure 15: Spectrometer image from the Argon measurements, with the x-scale converted into frequency with the reference spectrum in Fig. 13. The emission lines that were redirected and studied, and their energies, are indicated in the figure.

and 4.5 ± 0.5 meV for $3s3p^6 8p$, which can be translated into lifetimes according to:

$$\Delta E = \frac{h}{2\pi\tau} \quad \Leftrightarrow \quad \tau = \frac{h}{2\pi\Delta E} \tag{18}$$

where h is the Planck constant and ΔE is the linewidth in energy [13]. Using Eq. 18, the lifetimes that can be extracted from [18] is 98 ± 7.6 fs for $3s3p^6 7p$, and 146 ± 16 fs for $3s3p^6 8p$. It should be noted that this calculation assumes that the only broadening present is lifetime broadening and the instrumental broadening uncertainty given by the authors [18].

Identification of the Neon emission line could not be performed in the same way as the identification of the Argon emission lines, since not enough reference atomic lines could be found in the spectra. However, the evaluated emission line can be identified anyway. This is because the emission line is located close to another emission line, and the duo lies below the ionization potential (IP). This can be seen in Fig. 16; the decrease in intensity of the harmonics is seen to the right of the two emission lines. It can also be seen that the two emission lines are situated rather close to each other compared to the spacing between the odd harmonics, and only atomic lines typical for the Argon spectrum (and thus originate from the generation gas) can be seen below them, as indicated in the figure. From this, it can be concluded that the Neon emission lines probably correspond to $2s^2 2p^5 (^2P^0_{3/2}) 3s$ and $2s^2 2p^5 (^2P^0_{1/2}) 3s$, where the evaluated one is $2s^2 2p^5 (^2P^0_{3/2}) 3s$. The lifetime of this state has previously been measured to 23.6 ns [28].

4.3 Decay measurements

The decay measurements were performed according to the protocol described in Sec. 3, with the external voltage to the gas jet changing the ambient pressure between $2.0 \cdot 10^{-3}$ mbar, $3.8 \cdot 10^{-3}$ mbar and $5.4 \cdot 10^{-3}$ mbar for the Argon decay scans, while the ambient pressure was changed between $3.0 \cdot 10^{-5}$ mbar, $3.0 \cdot 10^{-4}$ mbar and $3.0 \cdot 10^{-3}$ mbar for the Neon decay scans. For all scans where an error log was saved (no error logs were taken during the first scan dates), the error log was

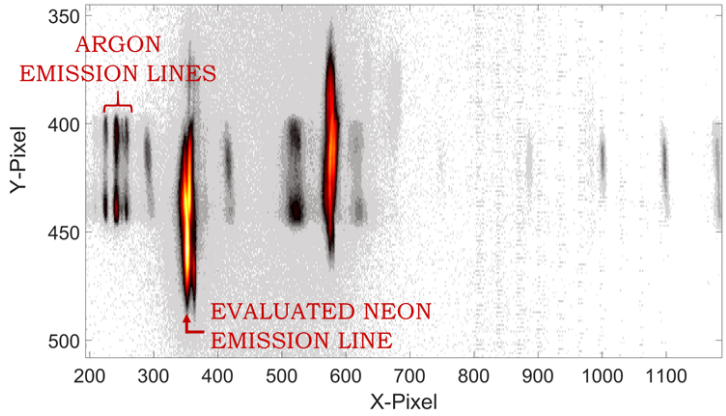

Figure 16: Spectrometer image used to identify the evaluated Neon emission line. The Argon emission lines and the emission line just to the right of the evaluated emission line were used to identify the Neon state that was studied. The Argon lines appear due to the High-order Harmonic Generation process, where Argon is used as the generation gas.

used to correct for any discrepancy between the expected position and the actual position of the translation stages.

The first method that was used to compensate for the intensity fluctuations was performed by normalizing against the on-axis radiation by division; the decay times measured with this technique are shown in Tab. 2 and Tab. 3.

Table 2: Measured decay times for the Argon emission lines, evaluated by normalizing the redirected intensity against the on-axis radiation.

	Argon ($3s3p^6 7p$)			**Argon ($3s3p^6 8p$)**		
Pressure [μbar]	**2.0**	**3.8**	**5.4**	**2.0**	**3.8**	**5.4**
2018-02-20	146 fs		480 fs	275 fs		703 fs
2018-02-21	147 fs	156 fs		331 fs	240 fs	
2018-02-22	267 fs			384 fs		
2018-03-05		322 fs	255 fs		596 fs	496 fs
2018-03-06	132 fs			273 fs		

Ideally, the values in each column of Tab. 2 and Tab. 3 should not differ from row to row, because only pressure changes should matter if the assumptions made in the proposed method hold. Clearly, the values differ significantly within the columns; the most extreme example being the Neon line at an ambient pressure of $3.0 \cdot 10^{-4}$ mbar, where the shortest extracted decay time and the longest differ by almost a factor of 10. Some of the results also suffer from a lack of consistency in the result of the fitting; for a discussion on this topic, the reader is directed to the appendix.

After the discovery that the results within the same column do not coincide, the rest of the project was dedicated to finding the root of these discrepancies. Several aspects of the proposed method were scrutinized to evaluate whether there is a hidden variable that changes between the scans, and if so, what the hidden variable is.

Table 3: Measured decay times for the Neon emission line, evaluated by normalizing the redirected intensity against the on-axis radiation. The measurements taken on the 19th of March were focused on evaluating the effect of the backing pressure of the gas jet, so for that date the backing pressure was set and measured. For dates marked with * the backing pressure was set to 2.0 bar, while ** denotes that the backing pressure was set to 4.0 bar.

	Neon ($2s^2 2p^5 (^2P^0_{3/2}) 3s$)		
Pressure [mbar]	$\mathbf{3.0 \cdot 10^{-5}}$	$\mathbf{3.0 \cdot 10^{-4}}$	$\mathbf{3.0 \cdot 10^{-3}}$
2018-03-06	252 fs		645 fs
2018-03-07	201 fs	280 fs	967 fs
2018-03-12		49 fs	296 fs
2018-03-16		33 fs	
2018-03-19*	140 fs		
2018-03-19**	127 fs		
2018-03-20	157 fs	53 fs	76 fs

First, the compensation for the laser fluctuations was removed in order to evaluate whether that could be the root of the discrepancies. A comparison was made of some of the decay times in Tab. 3 and the decay times obtained when no compensation was made in order to cancel out the intensity fluctuations of the laser; the result is shown in Tab. 4.

Table 4: Decay times from the decay measurements in Neon at an ambient pressure of $3.0 \cdot 10^{-5}$ mbar, where the decay times obtained with laser fluctuation compensation are compared to the decay times obtained without the laser fluctuation compensation.

	With fluctuation compensation			**Without fluctuation compensation**		
Date	**Scan 1**	**Scan 2**	**Scan 3**	**Scan 1**	**Scan 2**	**Scan 3**
2018-03-06	281 fs	243 fs	-	318 fs	242 fs	-
2018-03-07	192 fs	193 fs	190 fs	180 fs	195 fs	199 fs
2018-03-20	185 fs	168 fs	-	169 fs	173 fs	-

From Tab. 4 it can be seen that changing the fluctuation comparison does give a different result in some cases, but for most cases the decay time is similar and the discrepancy between different days remains.

The next two methods were evaluated in a slightly different way and more briefly. The first of the two is the method based on minimizing the correlation between the on-axis radiation and the redirected radiation that was described in the method section (Sec. 3.3). The results from this method were not satisfactory because the correlation clearly remained even after the attempt at minimizing it. This implies that a polynomial of higher order would have been necessary to remove the correlation. It was, however, not attempted to remove the correlation with a higher-order polynomial, as data manipulation using higher-order polynomials can be used to modify data to an extent where it can show practically anything.

The next fluctuation compensation that was attempted briefly was the deconvolution method described in the method section (Sec. 3.3), where the on-axis

radiation is used as a known noise signal that is removed by deconvolution. As promising as this method seemed at first, with the scenario almost being a textbook example of a known noise signal mixed in with the real signal, the method did not remove the correlation between the intensity fluctuations of the on-axis harmonics and the redirected radiation, and was therefore discarded.

The next evaluation was of the gas jet impact on the data. Ideally, one would want a stable pressure with a known pressure value and distribution at the spot where the laser beam excites the gas atoms. However, with the current setup that is not a possibility, so an analysis of the effect of gas pressure fluctuations on the data was performed.

The idea behind the analysis of the gas pressure fluctuations is to use the difference in absorption frequency for resonant and non-resonant radiation. Light that is not resonant with an atomic transition frequency should pass through the gas practically unaffected by pressure changes, while light that is resonant with an atomic transition should be absorbed and therefore strongly affected by pressure changes. This can be utilized by comparing harmonics below the IP with harmonics above the IP, since the harmonics above the IP are highly likely to interact with the gas particles and ionize them. Thus, any intensity fluctuation of the harmonics above the IP that is not matched by an intensity fluctuation in the harmonics below the IP could probably be attributed to pressure fluctuations. To evaluate whether the fluctuations were correlated, the ratio of the intensity of a below-IP harmonic to the intensity of an above-IP harmonic was evaluated. The result is given in Fig. 17a, and as seen in the figure, the pattern when the intensity of a harmonic below the ionization threshold is plotted against a harmonic above the ionization threshold seems random and no clear linearity can be seen. This seems to indicate that there is no correlation between the intensity fluctuations of the harmonics below the IP and the harmonics above it.

However, to make sure that this result was in fact an indication of that gas pressure fluctuations were important, the correlation between two harmonics below the ionization threshold, and between two harmonics above the threshold was evaluated. The result is given in Fig. 17c and Fig.17b. This result was truly surprising, since it was assumed that all harmonics except the one resonant with the redirected emission would be affected by the exact same optics in the same way, except for the interaction with the target gas where it was assumed that the harmonics above the ionization threshold would all be affected in one way and the harmonics below the ionization threshold would all be affected in another way; however, if this was the case, then the correlation patterns in Fig. 17c and Fig. 17b should have a clear, linear relation and not appear as random as they do in the figures.

Given the result in Fig. 17, it seems as though there is at least one process in the setup that affects different harmonics in different ways. A possible candidate for this process is the cutting of the beam with the iris before the stabilization and recombination chamber. To confirm this, the correlation evaluation method was changed so that only a smaller, intense part of the harmonics below and above the threshold was compared to find whether the intensity fluctuations were correlated or not. Since the most intense part is chosen and not the whole harmonic, possible differences in how the harmonics are cut by iris are minimized by this change of method. The result is presented in Fig. 18.

The correlation is, as seen in the increased linearity and decreased randomness

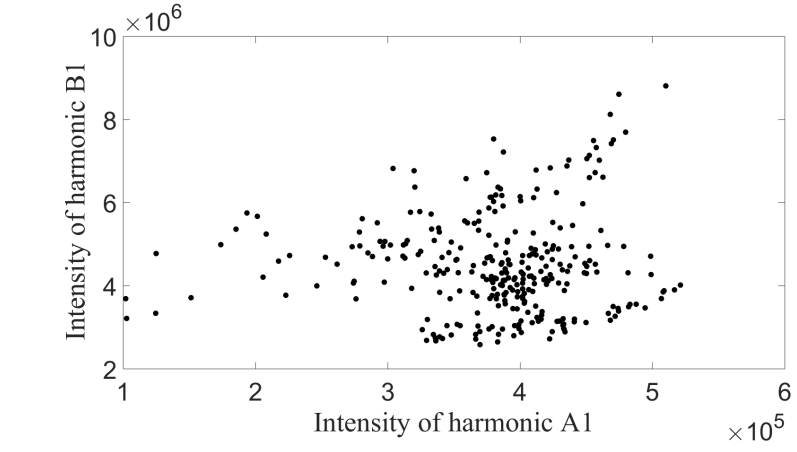

(a)

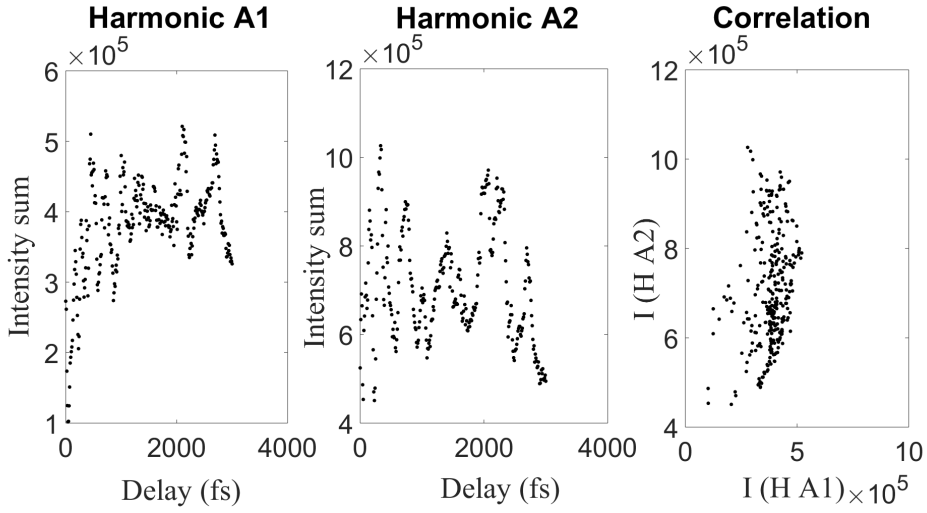

(b)

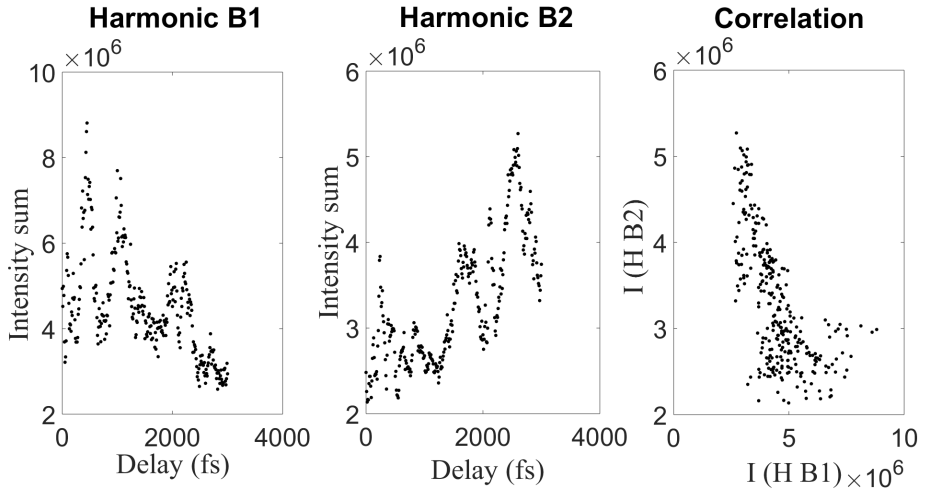

(c)

Figure 17: Investigation of the correlations between the intensity (I) fluctuations of a) a harmonic above and a harmonic below the ionization potential, b) two harmonics above the ionization potential, and c) two harmonics (H) below the ionization potential.

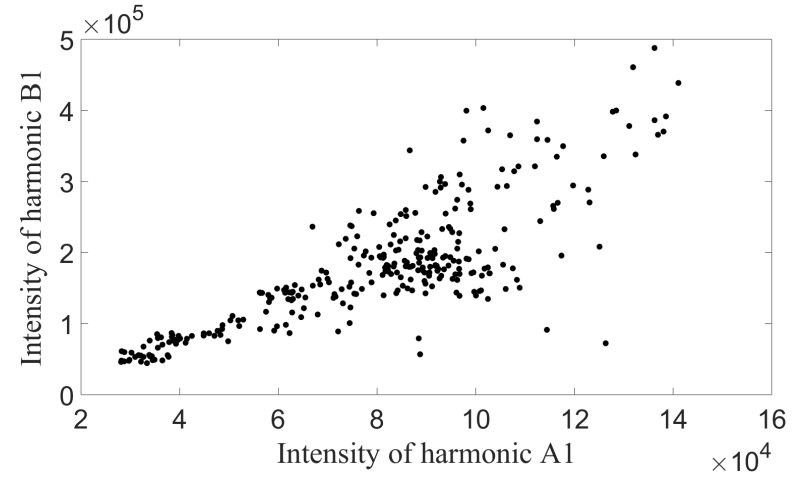

(a)

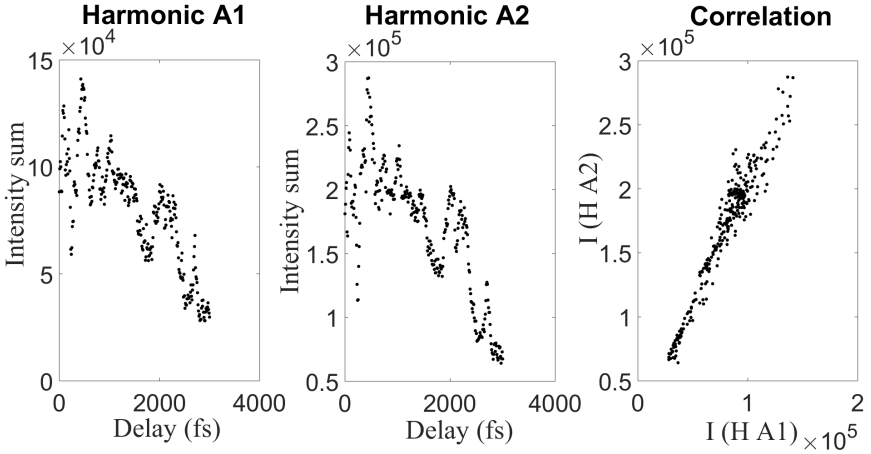

(b)

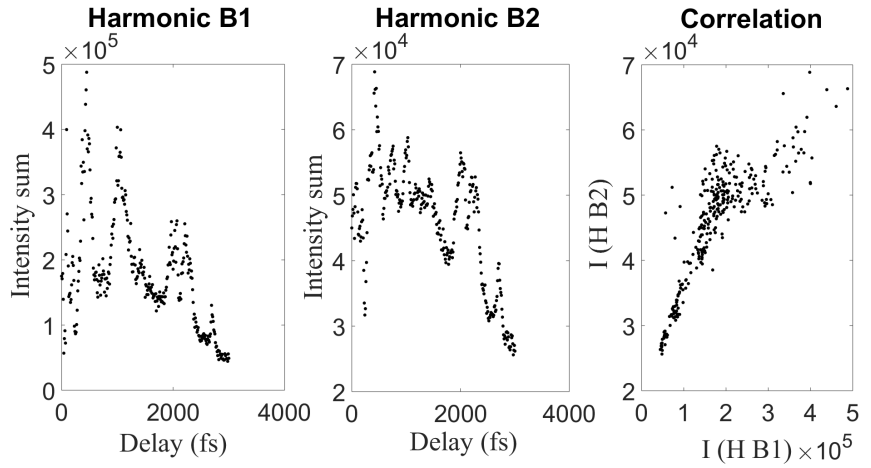

(c)

Figure 18: Investigation of the correlations between the intensity (I) fluctuations of the most intense parts of a) one harmonic below and one harmonic above the ionization potential, b) two harmonics above the ionization potential, and c) two harmonics (H) below the ionization potential.

of the patterns in Fig. 18c and Fig. 18b, clearer when only the intense parts of the harmonics are evaluated. This seems to confirm that the cutting of the harmonics affects each harmonic slightly differently, probably in that they do not keep the same area, and thus an integration over the whole harmonic is misleading. However, this different area should not affect the experiment as a whole, and given the clear correlation in Fig. 18a, the gas fluctuations does not seem to be an issue unless something is wrong with the assumptions leading up to the decision of checking for a possible gas fluctuation impact with a correlation comparison.

One final method for compensating for the fluctuations was evaluated; this was the method where it was assumed that the intensity of the adjacent harmonic and the redirected radiation should be constant, that is, the intensity of all pixels in the large shaded rectangle in Fig. 19 should be constant; therefore it is possible to look at the fraction of light that is redirected instead of direct values. This means that it is the fraction of the intensity of the pixels in the smaller rectangle in Fig. 19 to the intensity of the pixels in the large rectangle that is evaluated.

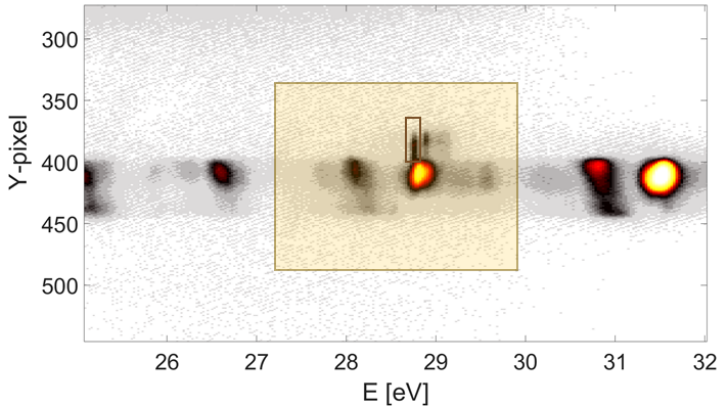

Figure 19: Spectrometer image from a decay measurement in Argon, where the large rectangle shows the pixel area where the pixel intensity sum is assumed to be constant throughout the measurement. The smaller rectangle shows the pixel area of the redirected light of the emission line that was evaluated.

This fraction method was applied to the same data as in Tab. 3, and the result is shown in Tab. 5. From the results, it can be seen that this method does not cancel out the discrepancies. However, the method does in general give very nice decay curves without any major fluctuations; an example is provided in Fig. 20a.

The fit to the data of Fig. 20a and the fit to the data in Fig. 20b seem at first sight good enough that the large difference in decay time between the two measurements would be affirmed. However, in Fig. 20c it can be seen that the fluctuations in Fig. 20b are in fact large enough to allow for a decent fit with an exponential decay of the same decay time as that of Fig. 20a. This result raises the question as to whether it is possible to perform this manual fitting for all measurements and find a decay time that is an acceptable fit for all of them. However, this seems unlikely, as the results in Tab. 5 are not substantially different from those in Tab. 3, which were obtained from multiple scans, taken back-to-back, which was thought to cancel out any ambiguity of the kind seen in Fig. 20.

Furthermore, if all discrepancies between scans with the same external parameters could be canceled out by manually adjusting the fitting parameters, it would

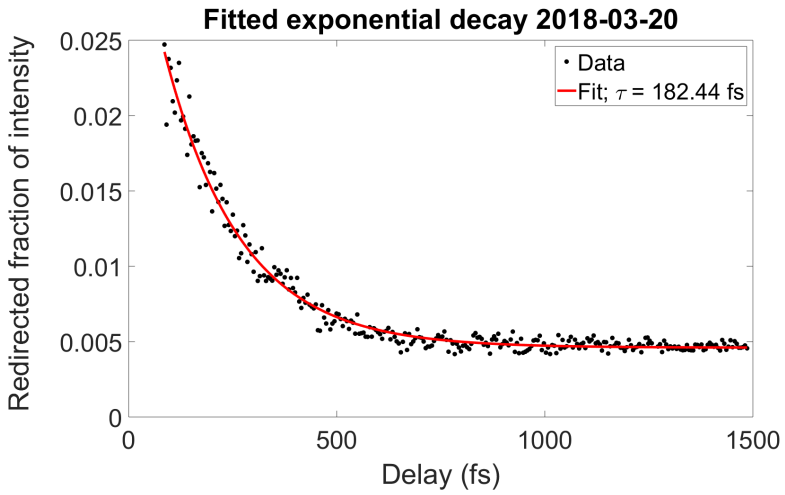

(a)

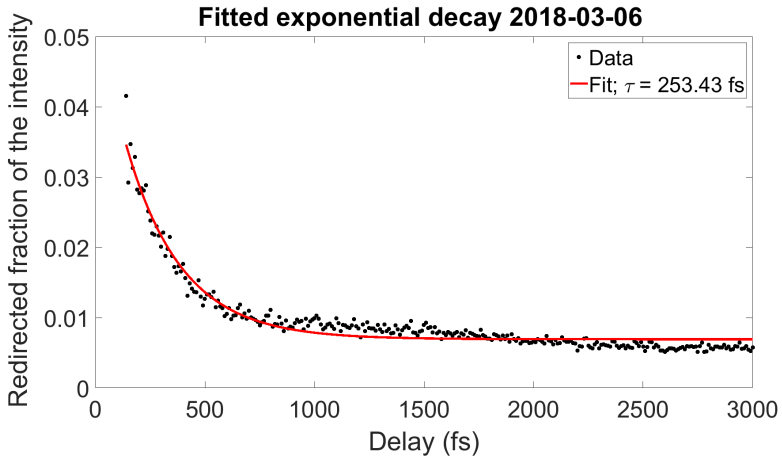

(b)

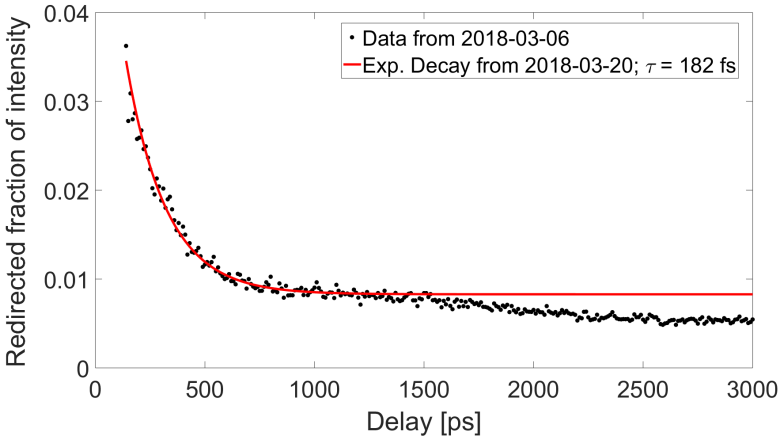

(c)

Figure 20: Experimentally measured redirected light from Neon atoms at an ambient pressure of $3.0 \cdot 10^{-5}$ mbar as a fraction of the total light of the adjacent harmonic, with a) an exponentially decaying function fitted to data from 2018-03-20, b) an exponentially decaying function fitted to data from 2018-03-06, and c) an exponential function with the same decay time as that of 2018-03-20 plotted on top of the data from 2018-03-06.

Table 5: The decay times of Neon calculated by evaluating the fraction of light that is redirected from a certain harmonic over time. For dates marked with * the backing pressure was set to 2.0 bar, while ** denotes that the backing pressure was set to 4.0 bar.

	Neon [$3.0 \cdot 10^{-5}$ mbar]		
Date	**scan1**	**scan2**	**scan3**
2018-03-06	285 fs	251 fs	-
2018-03-07	238 fs	201 fs	202 fs
2018-03-19*	166 fs	118 fs	125 fs
2018-03-19**	151 fs	128 fs	148 fs
2018-03-20	184 fs	174 fs	-

imply that the only thing needed to make the proposed method work is that the laser fluctuations must be decreased so that it would be possible to automate the process. An automated fitting process is absolutely necessary for speed and to avoid a subjective approach to the best fitting parameters. However, not all discrepancies between scans with the same external parameters could be canceled out. An example of an instance where even the manual fitting of the data cannot make two scans with the same parameters coincide is shown in Fig. 21. Here, the exact same approach as in Fig. 20 is applied, but the results from the two scans cannot in any physically significant way be made to coincide. This does not seem to be a mere coincidence, since the decay times extracted from the scans in Fig. 21a and Fig. 21b were both supported by the other scans in their respective sets.

These results invalidate the hypothesis that there might be consistent decay times for each pressure value, and instead indicate that there is another, unknown variable that was changed between the times the different measurements were taken. A candidate as to what this unknown variable may be is the actual pressure, or more exactly: where in relation to the gas jet outlets the beam is focused. This is something which could possibly change with the daily alignment of the laser, with the intensity of the laser, and with the daily drift of the laser. Fig. 22 shows what happens if the focus point would be moved for example from a point close to the gas outlet (point 1 in the figure) to a point further away from the outlet (point 2 in the figure): the gas has had a larger volume over which to disperse, and the effective pressure would be significantly decreased.

This hypothesis would perhaps be supported by the intensity modulation in Fig. 21a, which looks like it could be due to resonant pulse propagation as described in Sec. 2.2. Fig. 21b on the other hand, does not show the same modulation, indicating that the region from which the radiation in Fig. 21b was emitted had another density where RPP is not the dominant process.

Another effect that could possibly change the actual pressure in the interaction region is backing pressure changes. The reasoning behind this hypothesis is that the pulsed valve might inject more particles with a higher backing pressure, which would lead to pressure changes in the interaction region. However, the decay times did not change significantly between the scans taken with a backing pressure of 2.0 bar and those taken with a backing pressure of 4.0 bar, as seen in Tab. 5, which indicates that this effect is negligible.

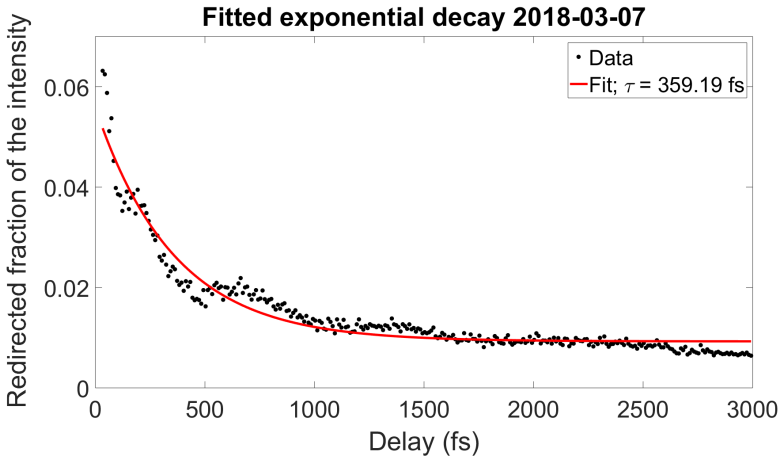

(a)

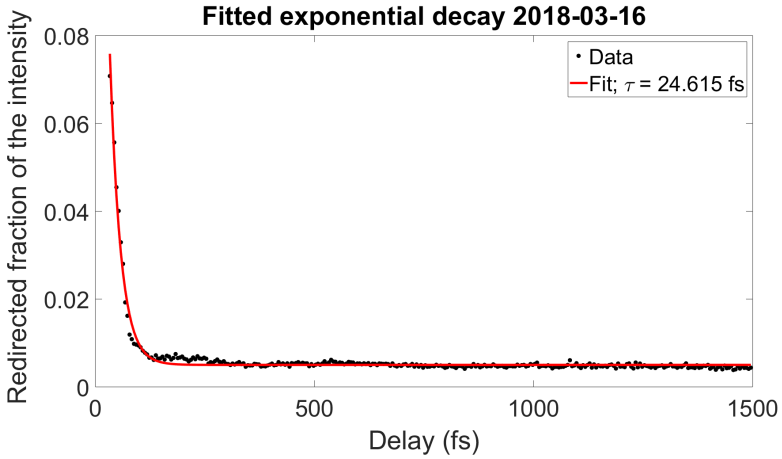

(b)

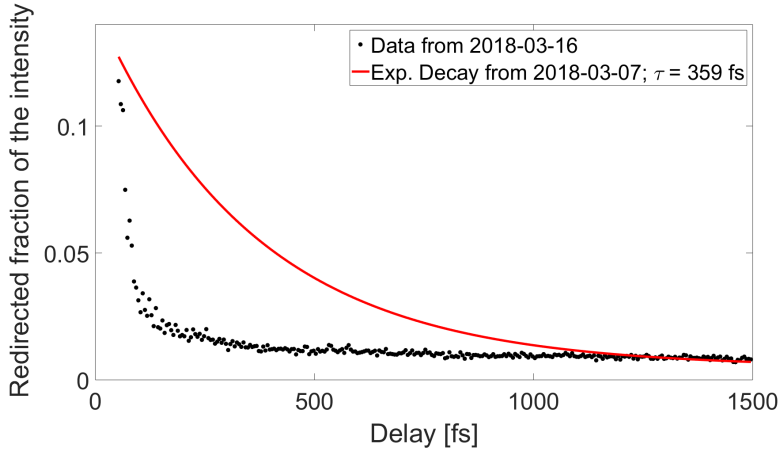

(c)

Figure 21: Experimentally measured redirected light from Neon atoms at an ambient pressure of $3.0 \cdot 10^{-4}$ mbar. The intensity of the redirected light is given as a fraction of the total light of the adjacent harmonic, with a) an exponentially decaying function fitted to data from 2018-03-07, b) an exponentially decaying function fitted to data from 2018-03-16, and c) an exponential function with the same decay time as that of 2018-03-07 plotted on top of the data from 2018-03-16.

(a) (b)

Figure 22: Schematic description of how the position of the focus may shift the gas pressure at the interaction point with the laser beam (red); for the case in a) the focus is close to the outlet and therefore the gas (blue) is dense where the laser beam interacts with the atoms, while the case in b) shows a focus that is located further away from the outlet and thus interacts with a gas that is less dense.

5 Outlook

The first thing that needs to be discussed is the large discrepancy between the obtained decay times and the previously measured lifetimes for the Neon emission line: the previously measured lifetime is 23.6 ns [28], a value that is much larger than any of the decay times obtained from the experiments in this thesis. This indicates that, even for the scans with the lowest ambient pressures, the influence of macroscopic effects was significant. For the Argon emission lines the previously measured lifetimes and the measured decay times were of about the same magnitude so the same reasoning cannot be made for these states, it should however be noted that all measured decay times were longer than the previously measured lifetimes. This is an unusual property and could be due to the fact that the Argon states are window resonances, which means that the impact of the macroscopic effects on the decay time is different for these states.

A possibility as to why there is such a large difference between the measured Neon decay times and the previously published lifetime, while the difference between the decay times obtained in this thesis and the lifetime published previously for the Argon measurements is much smaller, is that the Argon states are autoionizing, therefore the excitation cross-section is lower for these states than for the Neon state. This could lead to a lower density of excited atoms in the Argon measurements and thus less macroscopic effects. This theory might be supported by the fact that the Argon lines were more difficult to handle experimentally; it was difficult to find and redirect the emission lines, and once redirected, the redirected intensity was not significant in the same way it was for the Neon emission line. This behavior of the Argon lines seems to indicate less excited atoms in the gas.

As mentioned in the result section and as can be seen in Tab. 2, Tab. 3 and Tab. 5, the proposed method did not give consistent results. However, even though the results did not show the hoped-for possibility of measuring decay times and evaluating the effects on the decay time of pressure changes in the target gas, the result still hold importance in indicating what needs to be changed in the setup in order to proceed forward. There seems to be two main factors that made the results unreliable: the gas pressure uncertainty and the laser fluctuations. The laser fluctuations are what I personally would focus on first if improvements to the setup were to be made; the reason for this is that the non-linear processes involved seem to make the fluctuations impossible, or at least very difficult, to remove from the

data - and they hold no physical significance. Unfortunately, they are likely difficult to deal with since they originate from the laser source, hence it may be required to change the laser to be able to get a more stable intensity. If a laser change is to be made, there are during recent years examples of HHG being possible with certain turn-key lasers, that deliver a stable intensity [29].

The second large uncertainty was undoubtedly the gas pressure uncertainties. However, pressure effects on the emission spectrum is the physical phenomenon the proposed method sets out to evaluate, so even if they are not controllable or truly measurable, they still carry physical significance. If other uncertainty factors can be neglected, it can still be evaluated if the unknown pressure changes truly do have an impact on the resulting decay times the way Fig. 21 seems to imply, and if they do, how large is that impact? This would be a result in itself and give an indication on which aspects of a setup that are important to focus on if one wants to obtain higher levels of control of the light.

However, one aspect of the setup that seems important to change before any further experiments is the strong z-position-dependency of the laser focus discovered in Sec. 4.1, which adds to the uncertainty in the spatial relation between the gas jet and the beam focus. This uncertainty seems to make it near impossible to obtain consistent data over a longer timespan than a couple of hours. Since the manufacturing of gas jets has not been the focus for this project, it is difficult at this point to speculate in how to improve the gas pressure measurement and stability. A way to remove the sensitivity to the z-position of the beam focus might be to add more gas jets or an increased nozzle size with more outlets, creating a larger potential excitation area.

When it comes to data processing, it seems as though the method of looking at the fraction of the light that was redirected compared to that emitted in the forward direction gave the best conditions for further analysis and it is the method I would recommend for any future experiment similar to this one. This seems to imply that the assumption made in the method section (Sec. 3.3) is justified; the non-linearity of the HHG-process makes the XUV-light more sensitive to laser intensity fluctuations and the effect of the probe intensity fluctuations seems negligible in comparison to the effect of fluctuations of the XUV-light. Ideally, the fraction method should be combined with the precaution of taking multiple scans back-to-back and fitting the decay time with respect to all of them, as this provided better consistency in the results. For a discussion on the consistency of the results, see the appendix.

In a broader perspective, the result of this method evaluation is not a full step forward towards an OOM, but hopefully it will serve as a useful preparation for further attempts at intensity control of attosecond XUV light. It is worth highlighting how close this technique has come to fulfilling the request for a beamsplitter for ultrashort pulses: technically, the proposed method already manages to split the light into two different directions, which means that if the intensity ratio is not crucial, implementation might even already be possible. However, for a more general use, there are many steps left to be taken before the OOM is realized.

In conclusion, it does seem as though the numerous fields awaiting the advent of an OOM need to wait a bit longer before the optical counterpart to the AOM can have a chance at revolutionizing the pulse control possible for ultrashort pulses and XUV light in the same way the AOM did for longer timescales.

References

[1] D. Reid, R. Thomson, D. Faccio, C. Heyl, R. Trebino, G. Steinmeyer, H. Fielding, R. Holzwarth, P. Zhang, Z.and Del'Haye, T. Südmeyer, G. Mourou, T. Tajima, F. Harren, and G. Cerullo, "Roadmap on ultrafast optics.," *Journal of Optics*, vol. 18, no. 9, 2016.

[2] W.-C. Chu and C. D. Lin, "Photoabsorption of attosecond xuv light pulses by two strongly laser-coupled autoionizing states.," *Journal of physics B - Atomic, Molecular and Optical Physics*, 2012.

[3] A. McPherson, G. Gibson, H. Jara, U. Johann, T. S. Luk, I. A. McIntyre, K. Boyer, and C. K. Rhodes, "Studies of multiphoton production of vacuum-ultraviolet radiation in the rare gases," *J. Opt. Soc. Am. B*, vol. 4, no. 4, pp. 595–601, 1987.

[4] M. Ferray, A. L'Huillier, X. F Li, L. A Lompre, G. Mainfray, and C. Manus, "Multiple-harmonic conversion of 1064 nm radiation in rare gases," *Journal of Physics B: Atomic, Molecular and Optical Physics*, vol. 21, 1999.

[5] S. Bengtsson, *Ultrafast opto-optical control of extreme ultraviolet light pulses.* Lund University, 2017.

[6] D. R. Pape and A. P. Goutzoulis, *Design and fabrication of acousto-optic devices*. Taylor & Francis, 1994.

[7] S. Bengtsson, E. Larsen, D. Kroon, S. Camp, M. Miranda, C. Arnold, A. L'Huillier, K. Schafer, M. Gaarde, L. Rippe, and J. Mauritsson, "Space-time control of free induction decay in the extreme ultraviolet.," *Nature Photonics*, vol. 11, no. 4, pp. 252 – 258, 2017.

[8] L. Rippe, *Quantum computing with naturally trapped sub-nanometre-spaced ions.* Lund University, 2006.

[9] U. Fano and J. Cooper, "Spectral distribution of atomic oscillator strengths.," *Reviews of Modern Physics*, vol. 40, no. 3, pp. 441–507, 1968.

[10] R. P. Feynman, R. B. Leighton, and M. L. Sands, *The Feynman lectures on physics.* Reading, Mass. : Addison-Wesley, 1977.

[11] C. J. Foot, *Atomic physics.* Oxford master series in physics: 7, Oxford University Press, 2005.

[12] C. Ott, A. Kaldun, P. Raith, K. Meyer, M. Laux, J. Evers, C. H. Keitel, C. H. Greene, and T. Pfeifer, "Lorentz meets fano in spectral line shapes: a universal phase and its laser control," *Science*, vol. 340, no. 6133, pp. 716–720, 2013.

[13] B. E. A. Saleh and M. C. Teich, *Fundamentals of photonics.* Wiley series in pure and applied optics, Hoboken, N.J. : Wiley, cop., 2007.

[14] J. C. Toomay, *Radar principles for the non-specialist.* Scitech, 1998.

[15] C. Liao, A. Sandhu, S. Camp, K. Schafer, and M. Gaarde, "Attosecond transient absorption in dense gases: Exploring the interplay between resonant pulse propagation and laser-induced line-shape control," *Physical Review A - Atomic, Molecular, and Optical Physics*, vol. 93, no. 3, 2016.

[16] M. Wu, S. Chen, S. Camp, K. J. Schafer, and M. B. Gaarde, "Theory of strong-field attosecond transient absorption.," *Journal of physics B - Atomic, Molecular and Optical Physics*, vol. 49, no. 6, 2016.

[17] S. Zienau, "Optical resonance and two level atoms," *Physics Bulletin*, vol. 26, no. 12, p. 545, 1975.

[18] N. Berrah, B. Langer, J. Bozek, T. W. Gorczyca, O. Hemmers, D. W. Lindle, and O. Toader, "Angular-distribution parameters and r -matrix calculations of ar resonances," *Journal of Physics B: Atomic, Molecular and Optical Physics*, vol. 29, no. 22, p. 5351, 1996.

[19] A. Olofsson, *Population Oscillations in Excited Argon Atoms Initiated by Attosecond Pulses*. Lund University (Student Paper), 2016.

[20] E. Witting Larsen, *Attosecond Sources and Interferometers-Developments and Applications*. Lund University, 2016.

[21] K. Varjú, P. Johnsson, J. Mauritsson, A. L'Huillier, and R. López-Martens, "Physics of attosecond pulses produced via high harmonic generation," *American Journal of Physics*, vol. 77, no. 5, pp. 389–395, 2009.

[22] Attotech, 2013. `http://attotech.se/GR020.html`, accessed 2018-04-09.

[23] K. K. Seunarine and D. C. Alexander, "Chapter 6 - multiple fibers: Beyond the diffusion tensor," in *Diffusion MRI* (H. Johansen-Berg and T. E. Behrens, eds.), pp. 105 – 123, San Diego: Academic Press, 2014.

[24] J. Reader, C. Corliss, W. Wiese, G. Martin, and United States National Bureau of Standards and Center for Radiation Research, *Wavelengths and transition probabilities for atoms and atomic ions*. No. 1-2 in NSRDS-NBS, U.S. Dept. of Commerce, National Bureau of Standards, U.S. G.P.O., 1980.

[25] P. Palmeri and E. Biémont, "Energy levels of high- l states in neutral and singly ionized argon," *Physica Scripta*, vol. 51, no. 1, p. 76, 1995.

[26] L. Minnhagen, "Spectrum and the energy levels of neutral argon, Ar I," *J. Opt. Soc. Am.*, vol. 63, no. 10, pp. 1185–1198, 1973.

[27] S. Rae and K. Burnett, "Detailed simulations of plasma-induced spectral blueshifting.," *Physical Review A*, vol. 46, no. 2, pp. 1084 – 1090, 1992.

[28] Y. M. Aleksandrov, P. F. Gruzdev, M. G. Kozloz, A. V. Loginov, V. N. Makhov, R. V. Fedorchuk, and M. N. Yakimenko, "Oscillator-strengths of lines in neon absorption-spectrum in the 20-80 nm range," *Optika i Spektroskopiya*, vol. 54, no. 1, pp. 7–13, 1983.

[29] E. Lorek, E. W. Larsen, C. M. Heyl, S. Carlström, D. Paleček, D. Zigmantas, and J. Mauritsson, "High-order harmonic generation using a high-repetition-rate turnkey laser," *Review of Scientific Instruments*, vol. 85, no. 12, p. 123106, 2014.

List of Abbreviations

AOM Acousto-Optical Modulator

CCD Charge-Coupled Device

FWHM Full-Width at Half-Maximum

HHG High-order Harmonic Generation

IP Ionization Potential

IR Infra-red

MCP Microchannel Plate

OOM Opto-Optical Modulator

RPP Resonant Pulse Propagation

SNR Signal-to-Noise Ratio

XUV Extreme Ultraviolet

Appendix

Errors in the Fitting Process

The fitting process was performed mainly by least squares optimization. For the measurements where the least-squares method was unable to find a good fit, the built-in MATLAB optimization function PATTERNSEARCH was used for the optimization of the fitted exponential decay.

The error was calculated with the following expression:

$$\text{Error} = \frac{\sum |I_m - I_f|}{\sum I_m} \tag{19}$$

where I_m is the measured intensity and I_f is the intensity given by the fit. The absolute value of the residual for each time delay, $|I_m - I_f|$ was obtained from the FMINSEARCH function in MATLAB, and to make the errors comparable to each other the error was expressed in percentage of the sum of the measured intensities. These error values are sorted into tables in the same structure as in the report, with Tab. 6 corresponding to Tab. 2, Tab. 7 corresponding to Tab. 3, Tab. 8 corresponding to Tab. 4, and Tab. 9 corresponding to Tab. 5 in the report.

It should be stressed that this error is not calculated with respect to the obtained time delay, but with respect to how well the shape of the measured intensity signal coincides with an exponential decay.

Table 6: Error estimates for the exponential decay fits in Tab. 2, where decay times for the Argon emission lines are presented. The values in Tab. 2 were evaluated by normalizing the redirected intensity against the on-axis radiation.

	Argon Line 1			**Argon Line 2**		
Pressure [μbar]	**2.0**	**3.8**	**5.4**	**2.0**	**3.8**	**5.4**
2018-02-20	4%		14%	7%		10%
2018-02-21	6%	3%		5%	3%	
2018-02-22	6%			7%		
2018-03-05		9%	19%		10%	19%
2018-03-06	4%			6%		

The error estimates given in Tab:s 6-9 seem too small, as the result often changed significantly between different runs of the optimization. Granted, the error estimations treat the deviation from the exponential curve and are not error estimations of the decay time itself - but the decay time that is extracted from the fit can in some cases change drastically depending on which start values that are given to the optimization function. Such a drastic change does not seem to fit within the error margin. This could be because the fluctuations are in fact too large and irregular for the least-squares optimization to be sufficient and that a more advanced optimization routine, one that does not risk a false stop due to a local minimum, needs to be used. Therefore, the function PATTERNSEARCH was also evaluated. However, this function suffered from the same trait, that the output value changed significantly from run to run for certain measurements. When both of these issues are taken into account, it seems as though the fluctuations of the laser are simply too large for an automated optimization routine to be successful.

Table 7: Error estimates for the exponential decay fits in Tab. 3, where decay times for the Neon emission line are presented. The values in Tab. 3 were evaluated by normalizing the redirected intensity against the on-axis radiation. For dates marked with * the backing pressure was set to 2.0 bar, while ** denotes that the backing pressure was set to 4.0 bar.

	Neon		
Pressure [mbar]	$\mathbf{3.0 \cdot 10^{-5}}$	$\mathbf{3.0 \cdot 10^{-4}}$	$\mathbf{3.0 \cdot 10^{-3}}$
2018-03-06	11%		11%
2018-03-07	15%	15%	7%
2018-03-12		26%	18%
2018-03-16		16%	
2018-03-19*	13%		
2018-03-19**	11%		
2018-03-20	14%	21%	23%

Table 8: Error estimates for the exponential decay fits in Tab. 4, where decay times obtained without laser intensity fluctuation compensation are compared to the decay times that are obtained without the fluctuation compensation. The measurements from Tab. 4 were all taken at an ambient pressure of $3.0 \cdot 10^{-5}$ mbar.

	With fluctuation compensation			Without fluctuation compensation		
Date	**Scan 1**	**Scan 2**	**Scan 3**	**Scan 1**	**Scan 2**	**Scan 3**
2018-03-06	10%	10%	-	11%	11%	-
2018-03-07	13%	14%	14%	12%	16%	14%
2018-03-20	9%	7%	-	18%	12%	-

Table 9: Error estimates for the exponential decay fits in Tab. 5, where the decay times of a state in Neon obtained by evaluating the fraction of light that is redirected are presented. For dates marked with * the backing pressure was set to 2.0 bar, while ** denotes that the backing pressure was set to 4.0 bar.

	Neon [$\mathbf{3.0 \cdot 10^{-5}}$ mbar]		
Date	**scan1**	**scan2**	**scan3**
2018-03-06	10%	9%	-
2018-03-07	13%	13%	13%
2018-03-19*	5%	5%	5%
2018-03-19**	5%	5%	8%
2018-03-20	6%	5%	-

Another possibility is that the assumption of an exponential decay is too rough of an approximation for these signals. This could mean that the macroscopic processes that were discussed in the report affect the decay to an extent where the overall shape of the decay is changed significantly compared to the intrinsic exponential decay of a single decaying dipole oscillation. This hypothesis could be evaluated by changing the shape of the function that is optimized with respect to

the data into one where both an exponential decay and a polynomial, depending on the XUV-light intensity and the pressure, are incorporated.

The fraction method delivers graphs where the fluctuations seem smaller, yet the method suffers from the same issues with inconsistency of the output of the optimization. However, one method that delivers more consistent results is the method where duplicate scans are taken and then optimization is performed with all of the scans in the set taken into account. The method is not perfectly consistent, with some sets producing slightly different outputs from run to run, but it performs better than evaluation of single scans. Thus, it might be possible to obtain an automated optimization routine that gives consistent outputs for most measurements if the fraction method and the set method are combined. However, a more robust solution to this problem would be to find a way to reduce the laser fluctuations when the experiment is performed. Once again, this leads to the conclusion that this experiment would profit from a more stable laser to be able to provide consistent results.